

MAPPING THE EVOLUTION OF HIGH REDSHIFT DUSTY GALAXIES WITH SUBMILLIMETER OBSERVATIONS OF A RADIO-SELECTED SAMPLE

A. J. BARGER,^{1,2,3,4} L. L. COWIE,^{1,4} E. A. RICHARDS,^{2,4,5}

Accepted by the Astronomical Journal for the April 2000 issue

ABSTRACT

Direct submillimeter imaging has recently revealed the 850 μm background to be mostly composed of a population of distant ultraluminous infrared galaxies, but identifying the optical/near-infrared (NIR) counterparts to these sources has proved difficult due to the poor submillimeter spatial resolution. However, the proportionality of both centimeter and submillimeter data to the star formation rate suggests that high resolution radio continuum maps with subarcsecond positional accuracy can be exploited to locate submillimeter sources. In this paper we present results from a targeted SCUBA survey of micro-Jansky radio sources in the flanking fields of the Hubble Deep Field. The sources were selected from the uniform (8 μJy at 1σ) 1.4 GHz VLA image of Richards (1999b). Even with relatively shallow SCUBA observations (a 3σ detection limit of 6 mJy at 850 μm), we were successful at making submillimeter detections of optical/NIR-faint ($I \gtrsim 24$ and $K \simeq 21 - 22$) radio sources, and our counts closely match the bright counts from submillimeter surveys. An important corollary is that a large fraction of the bright (> 6 mJy) submillimeter sources in untargeted submillimeter surveys have extremely faint optical/NIR counterparts and hence are inaccessible to optical imaging and spectroscopy. However, redshift estimates can be made from the ratio of the submillimeter flux to the radio flux across the 100 GHz break in the spectral energy distribution. This procedure, which we refer to as *millimetric* redshift estimation, places the bright submillimeter population at $z = 1 - 3$ where it forms the high redshift tail of the faint radio population. The star formation rate density (SFRD) due to ultraluminous infrared galaxies increases by more than two orders of magnitude from $z \sim 0$ to $z \sim 1 - 3$. The SFRD at high redshift inferred from our > 6 mJy submillimeter observations is comparable to that observed in the ultraviolet/optical.

Subject headings: cosmology: observations — galaxies: distances and redshifts — galaxies: evolution — galaxies: formation — galaxies: active — galaxies: starburst

1. INTRODUCTION

Recent detections of distant dusty galaxies with the SCUBA camera (the Submillimeter Common User Bolometer Array; Holland et al. 1999) on the 15 m James Clerk Maxwell Telescope⁶ constitute a substantial fraction of the cosmic FIR background detected by the *FIRAS* and *DIRBE* experiments on the *COBE* satellite (Puget et al. 1996; Guiderdoni et al. 1997; Schlegel, Finkbeiner, & Davis 1998; Fixsen et al. 1998; Hauser et al. 1998; Lagache et al. 1999). Since the observed FIR background is comparable to the total unobscured emission at ultraviolet/optical wavelengths, a full determination of the global star formation history of the Universe requires a comprehensive understanding of this dust-enshrouded galaxy population. The 850 μm SCUBA surveys to date have reported galaxy number counts that are in general agreement (Smail, Ivison & Blain 1997; Barger et al. 1998; Hughes et al. 1998; Blain et al. 1999a; Eales et al. 1999; Barger, Cowie, & Sanders 1999); the cumulative surface density above 2 mJy is about $3 \times 10^3 \text{ deg}^{-2}$. The discrete sources have bolometric luminosities that are characteristically $\gtrsim 10^{12} h_{65}^{-2} L_{\odot}$ if they lie at $z \gtrsim 1$. More-

over, the sources for which measurements exist at multiple wavelengths (e.g. Ivison et al. 1998) show thermal spectral energy distributions (SEDs). Thus, the SCUBA sources are inferred to be the distant analogs of the local ultraluminous infrared galaxy (ULIG; Sanders & Mirabel 1996) population.

An essential observational goal is to determine the redshift distribution of the submillimeter population in order to trace the extent and evolution of obscured emission in the distant Universe. However, identifying the optical/NIR counterparts to the submillimeter sources is difficult due to the uncertainty in the SCUBA positions. Barger et al. (1999b) presented a spectroscopic survey of possible optical counterparts to a flux-limited sample of galaxies selected from the 850 μm survey of massive lensing clusters by Smail et al. (1998). Candidate optical counterparts in the SCUBA error-boxes were identified using moderately deep ground-based and *HST* exposures ($I \sim 23.5$ and $I \sim 26$, respectively). One-quarter of the sources could be reliably identified, and those had redshifts in the range $z \sim 1 - 3$. A lower limit of 20 per cent of the full sample showed signs of AGN activity. However, for the

¹Institute for Astronomy, University of Hawaii, 2680 Woodlawn Drive, Honolulu, Hawaii 96822

²Hubble Fellow

³Chandra Fellow at Large

⁴Visiting Astronomer, W. M. Keck Observatory, jointly operated by the California Institute of Technology and the University of California

⁵National Radio Astronomy Observatory & University of Virginia, 520 Edgemont Road, Charlottesville, VA 22903

⁶The JCMT is operated by the Joint Astronomy Center on behalf of the parent organizations, the Particle Physics and Astronomy Research Council in the United Kingdom, the National Research Council of Canada, and the Netherlands Organization for Scientific Research.

majority of the submillimeter sources there were either no optical counterparts or the optical associations were not secure. Such sources could either be at very high redshift or be so highly obscured that they emit their energy almost entirely in the submillimeter.

High resolution radio continuum maps with subarcsecond positional accuracy and resolution offer new opportunities for locating submillimeter sources and determining their physical properties. The unique advantage of centimeter and FIR observations is that galaxies and the intergalactic medium are transparent at these wavelengths, so observed flux densities are proportional to intrinsic luminosities. In galaxies without a powerful AGN, the radio luminosity is dominated by diffuse synchrotron emission from relativistic electrons accelerated in supernovae remnants from stars more massive than $8 M_{\odot}$. These massive stars live $\lesssim 3 \times 10^7$ yr; the relativistic electrons probably live $\lesssim 10^8$ yr (Condon 1992). Thus, radio observations probe very recent star formation. FIR observations of starburst galaxies are also a direct measure of massive star formation. As summarized by Condon (1992), radio continuum emission and thermal dust emission are empirically observed to be tightly correlated due to both being linearly related to the massive star formation rate. If the FIR-radio correlation applies to high redshift, as is plausibly the case (though at the very highest redshifts Compton cooling of the relativistic electrons by the microwave background may suppress the radio emission), then very sensitive radio observations can be used to pinpoint distant submillimeter sources.

In this paper we investigate the feasibility of using radio data to identify and characterize the bright submillimeter source population. Richards (1999b) recently obtained an extremely deep Very Large Array (VLA) 1.4 GHz image centered on the Hubble Deep Field (HDF). Richards et al. (1999) matched ground-based optical data from Barger et al. (1999a) to the radio image and found that ~ 20 per cent of the galaxies in the sample could not be identified to optical magnitude limits of $I \sim 25$. In other respects, such as radio size and spectral index, the optically-faint objects were not any different from the remaining population. Richards et al. (1999) proposed four possible scenarios to explain this population, including $1 < z < 3$ obscured starbursts (beyond $z \sim 3$ the sensitivity to star forming galaxies cuts off due to the flux density limits of the radio data), extreme redshift ($z > 6$) AGN, $z < 2$ obscured AGN, or one-sided radio jets.

In the first phase of our program we observed with LRIS on the Keck II 10 m telescope a complete subsample of the radio sources. Our primary objective was to determine the redshifts of the optical/NIR-faint ($HK' > 20.5$) radio sources. Although we were able to spectroscopically identify nearly all the objects in our subsample to $HK' \lesssim 20$ (all had $z \lesssim 1.3$), we were unable to obtain redshifts for the fainter objects. Either these sources are distant ($z > 1.5$) with spectral features lying outside the optical wavelength range, or the visibility of remarkable features is strongly affected by dust in the galaxies.

If the optical/NIR-faint radio sources are highly dust obscured systems, then it is possible that they will be detectable in the submillimeter. In the second phase of our program we observed with SCUBA 15 of the 22

optical/NIR-faint radio sources in the central ~ 80 square arcminute region of the radio map; another 4 were observed by Hughes et al. (1998; hereafter H98) in the HDF-proper. The jiggle map mode enabled simultaneous observations of a large fraction (31/48) of the optical/NIR-bright radio sources. Even with relatively shallow SCUBA observations (a 3σ detection limit of 6 mJy at $850 \mu\text{m}$), we detected 5 of the optical/NIR-faint radio sources; a sixth with submillimeter flux < 6 mJy was detected in the deep HDF-proper submillimeter map of H98. In contrast, none of the optical/NIR-bright radio sources were detected. We additionally detected two > 6 mJy sources that did not have radio counterparts. Thus, our targeted SCUBA survey of optical/NIR-faint radio sources turned up ~ 70 per cent of the bright submillimeter sources in our surveyed areas.

In the final phase of our program, we explored the feasibility of obtaining redshift estimates from the submillimeter-to-radio flux ratios, as recently suggested by Carilli & Yun (1999). We find that the redshifted Arp 220 SED reasonably describes both redshifted local ULIG data and known high redshift submillimeter sources and hence can be used as a rough redshift estimator. We estimate that all of our bright submillimeter sources fall in the redshift range $z = 1 - 3$, consistent with the redshifts for the lensed submillimeter sources of Barger et al. (1999b).

Once we have redshifts for the distant submillimeter source population, we can determine the global evolution of star formation in dust-obscured galaxies. Previous studies of the star formation rate density (SFRD) have primarily used rest-frame ultraviolet data (e.g. Madau et al. 1996). However, the ultraviolet emission from a galaxy is heavily affected by the presence of even small amounts of dust, and the extinction corrections are highly uncertain; for example, corrections for dust obscuration at $z \approx 3$ range from factors of ~ 3 (Pettini et al. 1997) to factors of ~ 15 (Meurer et al. 1997), though the more recent estimate of Meurer, Heckman, & Calzetti (1999) lowers the latter to a factor of ~ 5 . Only direct measurements of the reradiated light at submillimeter wavelengths can securely address the SFRD at high redshifts.

The true SFRD will receive contributions from both the ultraviolet/optical and the submillimeter. We find that the submillimeter contribution to the SFRD in the $z = 1 - 3$ range from our > 6 mJy sources is comparable to the observed ultraviolet/optical SFRD contribution. The ultraviolet Lyman-break galaxies are on the average undetected in the submillimeter at a 1σ level of ~ 0.5 mJy, and thus the Lyman-break galaxy population is largely distinct from the bright submillimeter population (Chapman et al. 1999). If we assume that fainter submillimeter sources have the same redshift distribution and properties as the > 6 mJy sample, then the SFRD of the entire population contributing to the submillimeter background is about an order of magnitude higher than the observed ultraviolet/optical SFRD. The contribution from ULIGs to the SFRD increases by more than two orders of magnitude from $z \sim 0$ to $z = 1 - 3$, which supports a scenario in which the distant submillimeter sources are the progenitors of massive spheroidal systems. This rapid evolution in the ULIG population sampled by SCUBA can be reproduced in models (e.g., Blain et al. 1999b,c).

In § 2 we present our radio sample and optical/NIR

imaging, along with our new SCUBA and LRIS observations. In § 3 we determine our radio-selected submillimeter source counts. In § 4 we introduce the predicted high redshift submillimeter-radio flux correlation and obtain millimetric redshift estimates for our sources. In § 5 we use the complementary information from radio and submillimeter fluxes to gain insights into the characteristics of our radio-selected submillimeter source population. In § 6 we compare the rest-frame colors of the radio sources that have spectroscopic redshifts with the rest-frame colors of our submillimeter sources and find that the latter are likely to fall in the extremely red object category. In § 7 we calculate the luminosities, number densities, and SFRDs of our submillimeter sources. We compare the submillimeter contribution to the SFRD with contributions from radio and ultraviolet/optical wavebands over a range of redshifts. In § 8 we summarize our main conclusions. We take $H_0 = 65 h_{65} \text{ km s}^{-1} \text{ Mpc}^{-1}$ and consider both $\Omega_M = 1$, $\Omega_\Lambda = 0$ and $\Omega_M = 1/3$, $\Omega_\Lambda = 2/3$, which should cover the full range of possible cosmologies.

2. SAMPLES AND OBSERVATIONS

The present study is based on deep radio maps centered on the HDF that were observed with the VLA at 1.4 GHz (Richards 1999b) and 8.5 GHz (Richards et al. 1998). The primary 1.4 GHz image covers a 40' diameter region with an effective resolution of $1.8''$ and a 5σ completeness limit of $40 \mu\text{Jy}$. The 8.5 GHz images have an effective resolution of $3.5''$ and a 5σ completeness limit of $8 \mu\text{Jy}$ over a radius of $\sim 1'$ from the HDF center, rising to $40 \mu\text{Jy}$ at $6.6'$.

The 1.4 GHz HDF map was trimmed to match the 79.4 arcmin² NIR and optical imaging of the field obtained by Barger et al. (1999a). The absolute radio positions are known to $0.1'' - 0.2''$ rms in the HDF; the alignment of the optical data to the radio data left residual astrometric uncertainties of $\sim 0.2''$ (Richards et al. 1999). There are 70 sources in our final radio sample.

Table 1 gives the 1.4 GHz radio catalog for the central 79.4 arcmin² region discussed above. The first five columns are catalog number, RA(2000), Dec(2000), 1.4 GHz radio flux, and radio flux uncertainty (Richards 1999b). The remaining columns, to be discussed in the following subsections, are HK' , I , V , R , B , and U' magnitudes, redshift, submillimeter flux, submillimeter flux uncertainty, and 6.75 and $15 \mu\text{m}$ ISOCAM fluxes (Aussel et al. 1999). The last column of Table 1 gives the radio spectral index α_r ($S \propto \nu^{\alpha_r}$) or limit for the sources where 8.4 GHz data are available and can be used to determine the origin of the radio emission (Richards 1999b). Inverted spectrum sources ($\alpha_r > 0$) invariably have self-absorbed synchrotron emission associated with an AGN. Flat spectrum sources ($-0.5 < \alpha_r < 0$) can be produced by AGN activity or by optically thin Bremsstrahlung radiation from star formation at higher radio frequencies ($\nu > 5 \text{ GHz}$). Steep spectrum sources ($\alpha_r < -0.5$) consist of diffuse synchrotron emission often associated with either radio jets or star formation in galaxies.

In this paper we use the radio spectral index as a crude discriminator between AGN and star formation activity. We arbitrarily classify any source with an available spectral index that has $\alpha_r > -0.3$ (there are six such sources in our sample) to be primarily powered by AGN activity.

2.1. Optical, Near-infrared, and Mid-infrared Imaging

Wide-field and deep HK' observations of the HDF and flanking fields were obtained using the University of Hawaii Quick Infrared Camera (QUIRC; Hodapp et al. 1996) on the 2.2 m University of Hawaii (UH) telescope and the 3.6 m Canada-France-Hawaii Telescope (CFHT). The HK' ($1.9 \pm 0.4 \mu\text{m}$) filter is described in Wainscoat & Cowie (in preparation); the empirical relation between HK' and K is $HK' - K = 0.13 + 0.05(I - K)$, which simplifies to $HK' - K = 0.3$, assuming the median $I - K$ galaxy color (Barger et al. 1999a). In Table 1 we use a 2σ limit of $HK' = 21.5$ for our wide-field image and a 2σ limit of $HK' = 22.6$ for our deep image in the area around the HDF proper.

Deep Johnson V and Kron-Cousins I -band observations were made with the CFHT over a much larger area using the UH8K CCD Mosaic Camera built by Metzger, Lupino, and Miyazaki. Details of the above HK' and optical observations can be found in Barger et al. (1999a). In Table 1 we use 2σ limits of $I = 25.3$ and $V = 26.4$.

In February 1998 we observed four of the sources in our radio sample with the near-infrared camera (NIRC; Matthews & Soifer 1994) on the Keck I 10 m telescope. These sources previously had only HK' limits but were detected in the NIRC observations. Conditions were photometric with seeing $\sim 0.7''$ FWHM. NIRC has a 256×256 InSb array with $0.15'' \times 0.15''$ pixels, giving a $38'' \times 38''$ field of view. We imaged at $2.1 \mu\text{m}$ (K') with total exposure times for each object of 3240 – 4320 s. The data were obtained in sets of 120 s exposures, and the center of the field was moved in a 3×3 grid pattern with $3''$ on a side. The centers of successive grids were moved by $2''$ between each set. A fifth source was subsequently detected with NIRC with a longer exposure under non-photometric conditions. The data were processed using median sky flats generated from the dithered images and calibrated onto the HK' images using other galaxies in the field.

We used the Low-Resolution Imaging Spectrometer (LRIS; Oke et al. 1995) on the Keck II 10 m telescope in March 1997 and February 1998 to obtain B -band and Kron-Cousins R -band images, respectively, of a strip region $6' \times 2.5'$ in size that crosses the HDF. The total exposure times were 1680 s and 1600 s for B and R , respectively, and the seeing was $0.8''$ in R and $1.3''$ in B . The 2σ limits are $B = 26.6$ and $R = 26.6$. Details of the observations can be found in Cowie & Hu (1998) and Cowie, Songaila, & Barger (1999).

Finally, a deep U' ($3400 \pm 150 \text{ \AA}$) image of an area 80 arcmin² centered on the HDF-proper was obtained using the ORBIT CCD on the UH telescope. The 2σ limit for the U' image is $U' = 25.8$. Details of the U' observations can be found in Wilson et al. (in preparation).

All photometric magnitudes were measured in $3''$ diameter apertures and then corrected to $6''$ diameter (near total) magnitudes following the procedures of Cowie et al. (1994).

Serjeant et al. (1997) obtained deep ISOCAM observations of the HDF and flanking fields at 6.75 and $15 \mu\text{m}$. The Aussel et al. (1999) reductions of the data produced a main source list of 49 objects (7σ) and a supplementary list of an additional 51 objects (3σ for $15 \mu\text{m}$ and 5σ for $6.75 \mu\text{m}$). Despite the large point spread function ($15''$ at

15 μm), in most cases the optical or NIR identification of the ISOCAM source was straightforward. The redshifts for sources in the sample are in the range $z = 0.078$ to $z = 1.242$ (median $z = 0.585$).

2.2. Keck Spectroscopy

We used LRIS during a two night run on Keck II in March 1999 to obtain spectroscopic observations of a subsample of the 1.4 GHz sources in a strip region centered on the HDF. Although the HDF and flanking field region has been intensely studied by a number of groups (see Cohen et al. 1999 for a summary and references), most of the sources in our sample had not been previously observed due to their faint optical fluxes. We used 1.4'' wide slits and the 400 lines mm^{-1} grating blazed at 8500 Å, which gives a wavelength resolution of ~ 12 Å and a wavelength coverage of ~ 4000 Å. The wavelength range for each object depends on the exact location of the slit in the mask but is generally between ~ 4000 and 10000 Å. Three of the slit masks were constructed at a position angle of 90° , and the remaining three were nearly identical versions constructed at a position angle of -90° . This procedure enabled us to obtain sufficient wavelength coverage for all the objects in our sample, including those that fell close to the edges of the masks. The observations were 1.5 hr per slit mask, broken into three sets of 30 minute exposures. Three HDF slit masks were observed per night. Some of the objects were in all of the slit masks and hence were observed for 9 hrs (see Table 2). Conditions were photometric with seeing $\sim 0.6'' - 0.7''$ FWHM both nights. The objects were stepped along the slit by $10''$ in each direction, and the sky backgrounds were removed using the median of the images to avoid the difficult and time-consuming problems of flat-fielding LRIS data. Details of the spectroscopic reduction procedures can be found in Cowie et al. (1996).

In Table 2 we list all the objects in the radio sample that fall in the LRIS strip region. The columns are radio catalog number from Table 1, HK' mag, I mag, redshift, and exposure time for any object targeted in our March 1999 spectroscopic survey. Over an area ~ 58 arcmin², 19 of the 37 radio sources now have secure redshift identifications; all are at $z \lesssim 1.3$. Figure 1a, b shows HK' versus redshift and I versus redshift. Spectroscopic redshifts are in general relatively straightforward to obtain for radio objects with $HK' \lesssim 20$.

We note that Waddington et al. (1999) claim a redshift identification of $z = 4.42$ for object 30 based on a Ly α detection. However, the position of their detection is $1''$ away from the radio source position and counterpart optical galaxy, and so an association with the radio source is not secure. The radio source is detected in the mid-IR, which would suggest $z < 1.3$, consistent with the redshift estimated using the millimetric redshift technique described in § 4. However, we did not see any strong [O II] 3727 feature in our spectrum from 4000 – 9200 Å, which would suggest $z > 1.5$. Thus, the redshift of this object remains uncertain.

In all of our slit-masks (equivalent to a 9 hr integration) we also included the position of the brightest SCUBA source, HDF850.1, from the deep 850 μm map of the HDF-proper by H98. We centered our slit across the position of the 1.3 mm detection of HDF850.1 reported by Downes et

al. (1999), which also coincides with the 8.5 GHz supplemental radio source 3651+1226 (Richards et al. 1998). We oriented the slit such that it fell across both the arc-like feature 3-593.0 that is favored by Downes et al. (1999) as the optical counterpart to HDF850.1 and the nearby red galaxy 3-586.0. However, we were unable to determine a secure redshift for either source from our spectroscopic data.

2.3. Submillimeter Observations

Our SCUBA jiggle map observations were flexibly scheduled in mostly excellent observing conditions during two runs in April and June 1999 for a total of five observing shifts. The maps were dithered to prevent any regions of the sky from repeatedly falling on bad bolometers. The chop throw was fixed at a position angle of 90° so that the negative beams would appear 45 arcsec on either side east-west of the positive beam. The data were reduced using beam weighted extraction routines that included both the positive and negative portions of the chopped images, thereby increasing the effective exposure times. Regular “skydips” (Lightfoot et al. 1998) were obtained to measure the zenith atmospheric opacities at 450 and 850 μm , and the 225 GHz sky opacity was monitored at all times to check for sky stability. The median 850 μm optical depth for all nights together was 0.265. Pointing checks were performed every hour during the observations on the blazars 0954+685, 1418+546, 0923+392, or 1308+326. The data were calibrated using 30 arcsec diameter aperture measurements of the positive beam in beam maps of the primary calibration source, Mars, and one of three secondary calibration sources, CRL618, IRC+10216, or OH231.8.

The data were reduced in a standard and consistent way using the dedicated SCUBA User Reduction Facility (SURF; Jenness & Lightfoot 1998). Due to the variation in the density of bolometer samples across the maps, there is a rapid increase in the noise levels at the very edges. We have clipped the low exposure edges from our images. We present our SCUBA maps in Fig. 2.

We also re-reduced the archival HDF-proper SCUBA data of H98 in order to make a consistent analysis with the present data. We could only make use of the maps that were taken with a fixed RA chop (90 per cent of the data sample), which included 34 hours with a 30 arcsec chop throw and 28 hours with a 45 arcsec chop throw. We combined these data separately to form two independent maps. In Table 1 we quote submillimeter fluxes determined from the weighted average of measurements made in each map.

The SURF reduction routines arbitrarily normalize all the data maps in a reduction sequence to the central pixel of the first map; thus, the noise levels in a combined image are determined relative to the quality of the central pixel in the first map. In order to determine the absolute noise levels of our maps, we first eliminated the $\gtrsim 3\sigma$ real sources in each field by subtracting an appropriately normalized version of the beam profile. We then iteratively adjusted the noise normalization until the dispersion of the signal-to-noise ratio measured at random positions became ~ 1 . Our noise estimate includes both fainter sources and correlated noise.

We centered on the positions of the radio sources and measured the submillimeter fluxes in both the positive

TABLE 2
1999 MARCH KECK II LRIS SPECTROSCOPIC OBSERVATIONS

#	HK'	I	Redshift	Exposure (hr)
16	23.39	25.30	...	6
17	18.75	22.49	1.013	9
23	16.36	19.09	0.456	...
24	19.10	22.29	1.219	...
25	19.25	22.71	...	3
26	22.29	25.30	...	6
28	21.22	25.30	...	6
30	21.23	25.30	...	3
31	18.06	20.86	0.857	...
32	17.85	21.04	1.013	...
33	21.65	24.72	...	3
35	18.36	20.76	0.961	...
36	22.60	25.30	...	3
37	21.00	23.20	...	3
38	18.74	21.09	0.475	...
40	17.36	19.88	0.410	...
41	21.50	25.30
42	16.52	18.70	0.321	...
43	19.31	21.88	1.275	...
44	21.50	25.30	...	6
46	22.60	25.30	...	9
47	19.55	22.64	0.474	...
48	18.52	20.92	0.761	...
50	20.14	24.81	0.884	...
51	19.21	21.89	1.243	...
52	18.18	20.55	0.902	...
53	20.29	24.70	...	3
54	20.76	25.13	...	3
56	17.98	19.87	0.422	...
59	19.51	22.66	...	3
60	20.08	22.90	...	6
61	20.38	22.90
62	17.36	19.80	0.558	...
64	17.59	19.90	0.411	7.5
65	20.90	25.30	...	3
66	19.39	22.14	1.019	3
69	21.50	25.30	...	1.5

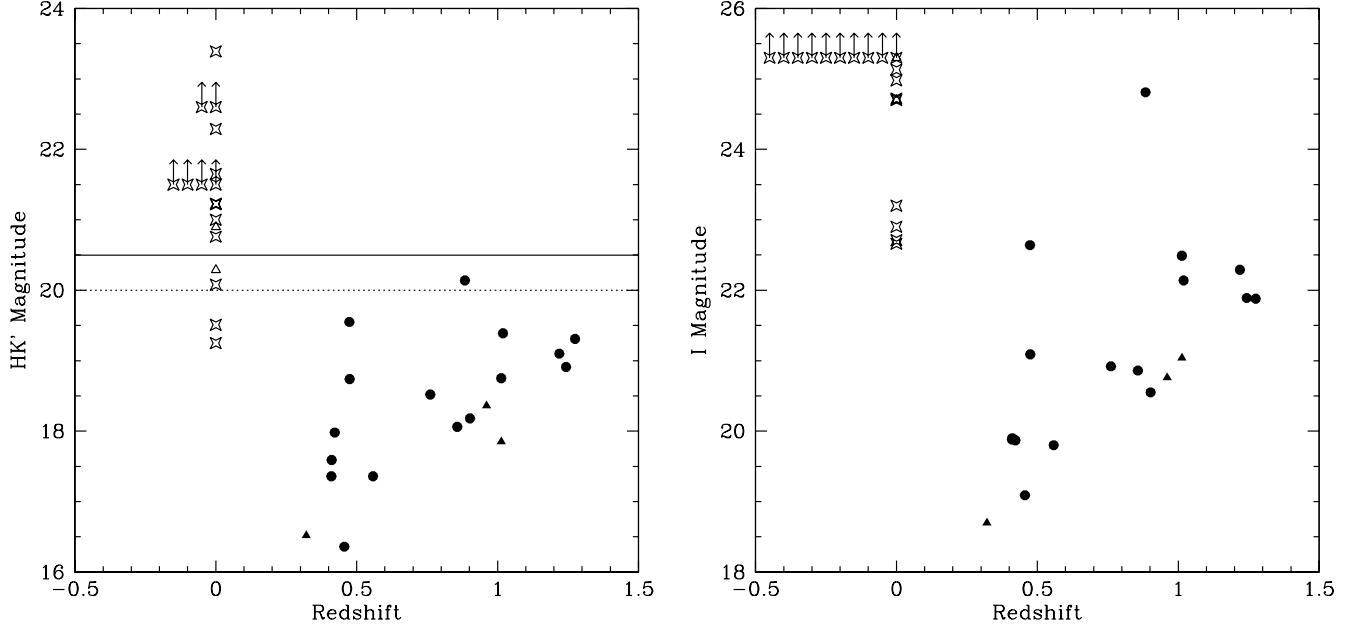


FIG. 1.— (a) HK' and (b) I versus redshift for our LRIS sample. Magnitude limits are indicated by arrows. Open symbols at $z \lesssim 0$ do not have redshifts. Triangles have spectral indices > -0.3 , indicating AGN. Dotted line in (a) at $HK' = 20$ is the practical spectroscopic limit. Solid line at $HK' = 20.5$ is our bright magnitude bound to the optical/NIR-faint radio sample (see §2.3).

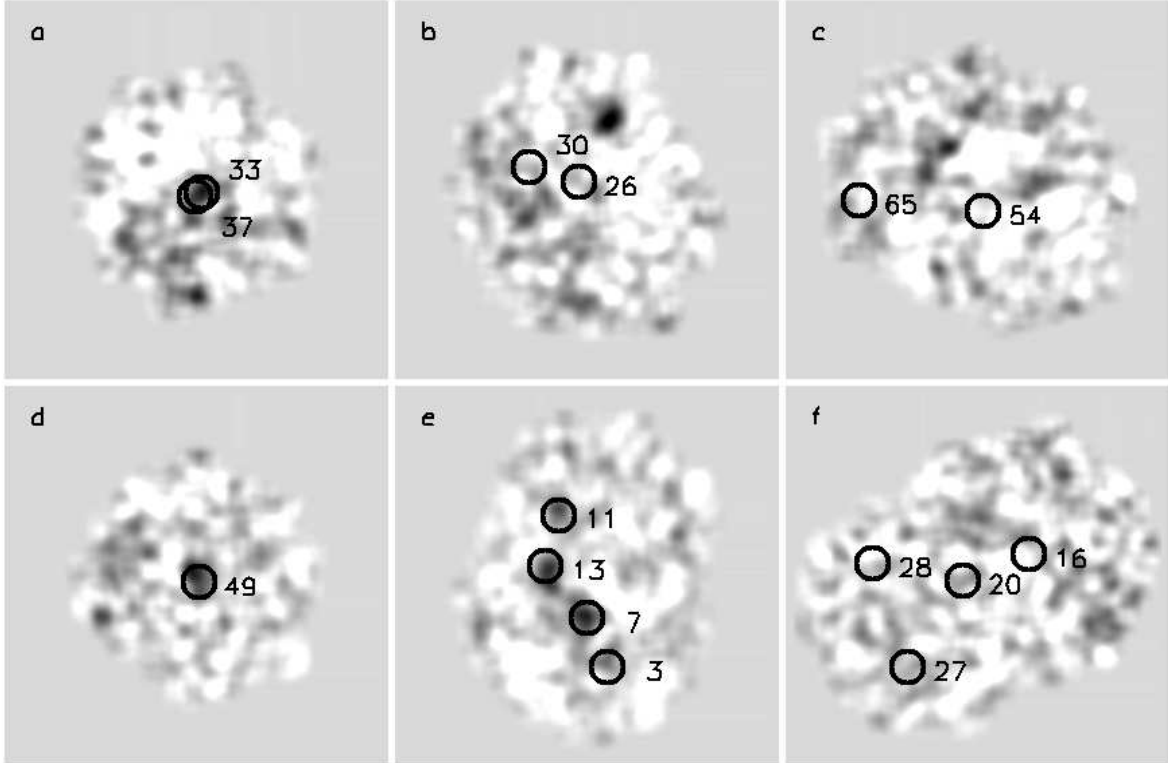


FIG. 2.— 850 μm SCUBA maps of our 6 radio-selected fields (excluding the H98 map) overlaid with circles at the positions of all optical/NIR-faint 1.4 GHz sources. North is up and East is to the left in the images. Labels are the catalog numbers from Table 1 for the optical/NIR-faint sources.

and negative beams. The extracted fluxes were calibrated to the 30 arcsec diameter aperture fluxes of the brightest sources. The brighter submillimeter sources were sub-

tracted from the maps before the fainter sources were extracted. In cases where the positions of two radio sources are very close, we may be slightly overestimating the sub-

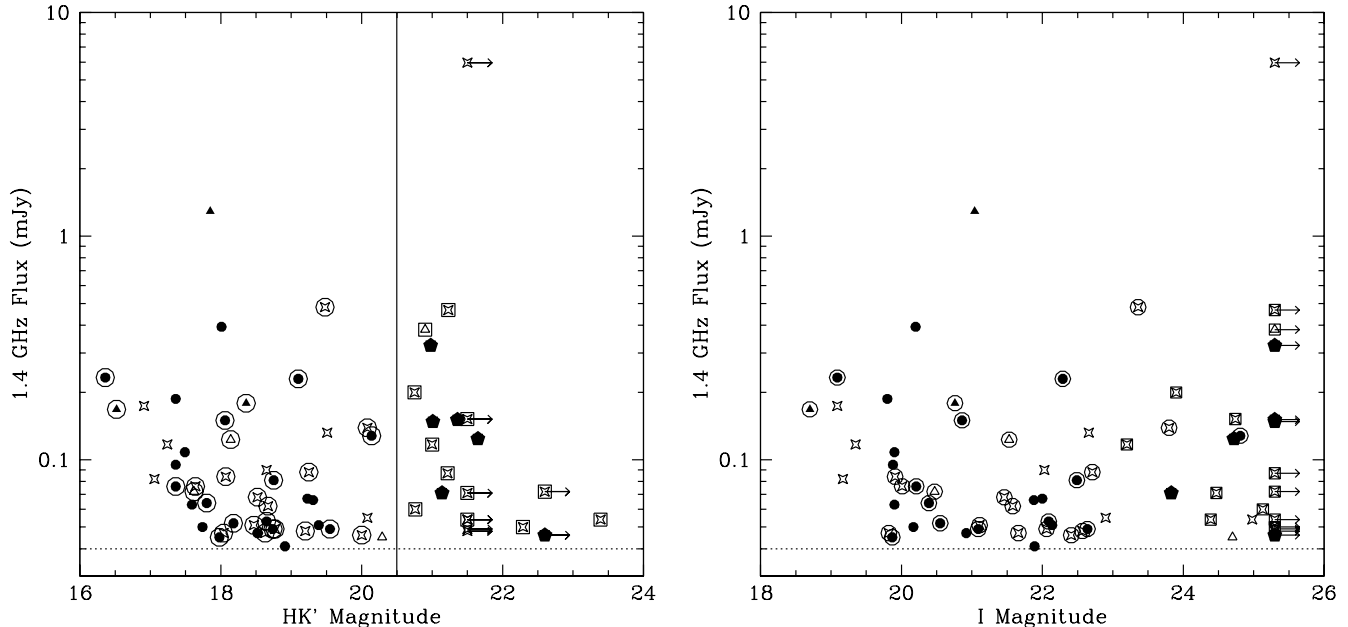


FIG. 3.— 1.4 GHz flux versus (a) HK' and (b) I mag for our radio sample. Filled circles have known redshifts (all are at $z < 1.3$); open crosses do not. Filled (known redshifts) and open triangles have $\alpha_r > -0.3$. Open circles were observed at 353 GHz (850 μm) but not detected at the typical 6 mJy (3σ) level. Filled pentagons have submillimeter detections. Dotted horizontal line is the 1.4 GHz flux limit of 0.040 mJy. Vertical line in (a) is our $HK' = 20.5$ optical/NIR-faint radio source bright magnitude limit.

millimeter flux allocated to the bright source with this procedure and underestimating that allocated to the faint source, but since the total submillimeter flux should be reasonable, we will not be making any gross errors in our later estimates of the total star formation rate.

From the total sample of 70 radio-selected galaxies in the ~ 80 square arcminute central region of the radio map, we take the 22 with $HK' > 20.5$ to be our optical/NIR-faint radio sample, for which there are now submillimeter observations of 19. Even though our SCUBA observations were relatively shallow (the 850 μm 3σ limit was 6 mJy), we detected 5 of the 15 optical/NIR-faint radio sources that we observed; a sixth significant source ($S_{850\mu\text{m}} = 2.4 \pm 0.7$ mJy) was detected in the HDF-proper SCUBA map of H98 (HDF850.2 in their notation). The submillimeter flux we measure for the brightest source (HDF850.1) in the HDF-proper map is 5.4 ± 0.6 mJy, which is slightly lower than the value of 7.0 ± 0.4 found by H98 but is consistent within the statistical and systematic errors. The jiggle map observing mode enabled simultaneous observations of a large fraction (31/48) of the optical/NIR-bright radio sources, none of which were detected. There are two > 6 mJy submillimeter sources in our jiggle maps that were not in the radio sample.

In Fig. 3a, b we show the 1.4 GHz fluxes of the radio sources in our sample versus their HK' and I magnitudes, indicating those with measured redshifts and those with submillimeter detections.

3. SUBMILLIMETER SOURCE COUNTS

We find that the radio selection technique is effective in locating the majority of bright submillimeter sources. We document this in Fig. 4 where we compare the combined 850 μm source counts from blank field submillimeter sur-

veys (H98; Eales et al. 1999; Barger, Cowie, & Sanders 1999) with our new radio-selected 850 μm source counts. A source of flux strength S_i contributes $N(S_i) = 1/A_i$ to the counts per unit area, where A_i is the area over which there is $\geq 3\sigma$ sensitivity to S_i . The cumulative counts, $N(> S)$, are given by the sum of the inverse areas of all sources brighter than S . However, for our radio-targeted search, the effective area (65 square arcminutes) is greater than if we had done an untargeted search with the same number of pointings and is given by the fraction (number $HK' > 20.5$ sources observed)/(total number $HK' > 20.5$ sources in sample) times the radio survey area (79.4 square arcminutes). Because of the correspondence between the optical/NIR-faint radio population and the bright submillimeter population, we do not need to survey the entire radio field in order to observe the bright submillimeter population.

It is interesting to speculate whether the correspondence between optical/NIR-faint radio sources and bright submillimeter sources also holds at fainter submillimeter flux levels. A necessary requirement for this to be the case is that the surface density of faint radio sources be comparable to or exceed the surface density of submillimeter sources. Extrapolating a power-law parameterization of the 1.4 GHz counts over the range $40 - 1000 \mu\text{Jy}$ (Richards 1999b) down to a $1 \mu\text{Jy}$ cut-off gives $N(S_{1.4} > 1 \mu\text{Jy}) = 127 \text{ arcmin}^{-2}$. The empirically estimated surface density of submillimeter sources (Barger, Cowie, & Sanders 1999) is $N(S_{353} > 0) \simeq 11 \text{ arcmin}^{-2}$.

A possible counter-argument to a close correspondence between radio and submillimeter sources at faint submillimeter flux levels comes from the study by Smail et al. (1999b) who compared their lensed submillimeter survey data with radio data. They found that the Carilli &

Yun (1999) radio-submillimeter spectral indices differed for their bright and faint submillimeter subsamples. They suggested that the difference could arise if the faint submillimeter sources lie at higher redshifts or have different fractions of radio-loud AGN or have different dust temperatures. However, with the low statistics, strong conclusions cannot be drawn at this time.

4. MILLIMETRIC REDSHIFT ESTIMATION

Optical spectroscopic surveys of submillimeter galaxies are difficult because of the very different behaviors of the K -corrections in the optical and submillimeter and the poor submillimeter resolution. Spectroscopic surveys to date (Barger et al. 1999b; Lilly et al. 1999) give potentially conflicting results and are very limited in size. Photometric redshift estimates of submillimeter sources have been made from candidate optical counterparts (H98; Lilly et al. 1999), but these are questionable both because the counterpart identification is not secure and because the SEDs of the submillimeter sources may be unlike those of the optical sources used in making the redshift estimates due to dust extinction and possible AGN contributions. Consequently, a new approach is required if the positions of the submillimeter sources are to be reliably determined and their nature and redshift distribution understood.

The remarkably tight local correlation between the global FIR and nonthermal radio luminosities provides a promising alternative method for identifying and studying individual submillimeter sources, provided that the correlation holds to high redshift. In § 3 we found that targeting with SCUBA optical/NIR-faint 1.4 GHz sources is an efficient technique for identifying the majority of the bright submillimeter source population. Our results indicate that a large fraction of bright sources in submillimeter surveys have extremely faint optical/NIR counterparts and hence are inaccessible to optical spectroscopy (see also Smail et al. 1999b). This conclusion is consistent with results from the Barger et al. (1999b) spectroscopic survey of lensed submillimeter sources discussed in the introduction.

Although we are unable to obtain spectroscopic redshifts for the optical/NIR-faint radio-selected submillimeter sources, we can use the submillimeter-to-radio flux ratios to obtain millimetric redshift estimates. Figure 5 illustrates how the slope of a dusty galaxy's SED changes abruptly at frequencies higher than 100 GHz. Below 30 GHz synchrotron radio emission is dominant, free-free emission is largest in the range 30 – 200 GHz, and thermal dust emission dominates above 200 GHz. Because of the opposing spectral slopes of the blackbody spectrum in the submillimeter and the synchrotron spectrum in the radio, the submillimeter-to-radio flux ratio rises extremely rapidly with increasing redshift (see Fig. 6). Carilli & Yun (1999; hereafter CY99) have therefore suggested using the submillimeter-to-radio flux ratio as a redshift estimator.

The dust emission from local luminous infrared galaxies is well described by optically thin single-temperature modified blackbodies with extinction coefficient $\epsilon_\nu \propto \nu^\beta$, where $\beta \approx 1$ to 2. The dust temperatures derived lie between 30 and 60 K. Arp 220, with its high bolometric luminosity produced almost entirely from starburst activity (Downes & Solomon 1998), is an appropriate prototype for high redshift submillimeter sources, as we will justify subsequently. Over the interval $100 \text{ GHz} \lesssim \nu \lesssim 10^4 \text{ GHz}$

($3000 \mu\text{m} \gtrsim \lambda \gtrsim 30 \mu\text{m}$) Arp 220's SED is well represented by a modified blackbody with $\beta = 1$ and a dust temperature $T_d = 47 \text{ K}$; the luminosity of this dominant cooler component is $1.36 \times 10^{12} h_{65} \text{ L}_\odot$ (Klaas et al. 1997). In terms of the blackbody distribution

$$B(\nu, T) = \frac{S(\nu, T)}{\pi} = \frac{2h\nu^3}{c^2} \frac{1}{e^{h\nu/kT} - 1} \quad (1)$$

the submillimeter flux for an Arp 220-like galaxy at redshift z is given by

$$S_s = f(0.57 \text{ Jy}) \pi B(\nu(1+z), T_d) \nu^\beta (1+z)^{1+\beta} \left[\frac{d_L(z_{\text{Arp}})}{d_L(z)} \right]^2 \quad (2)$$

where ν is the observed submillimeter frequency, T_d is the dust temperature, and d_L is the luminosity distance. We allow for an overall strength factor, f , relative to Arp 220, for which $f = 1$. The above normalization constant is fixed by a χ^2 fit to the Arp 220 flux measurements. In the Rayleigh-Jeans long-wavelength limit, the submillimeter flux is approximately given by

$$S_s = f(0.825 \text{ Jy})(1+z)^{1+\alpha_s} \left(\frac{T_d}{47 \text{ K}} \right) \left(\frac{\nu}{375 \text{ GHz}} \right)^{\alpha_s} \left[\frac{d_L(z_{\text{Arp}})}{d_L(z)} \right]^2 \quad (3)$$

which is normalized to the measured 375 GHz (800 μm) flux value for Arp 220 from Rigopoulou, Lawrence, & Rowan-Robinson (1996); here $\alpha_s = \beta + 2 = 3$. The approximation in Eq. 3 is reasonably accurate for $z \lesssim 3$; at higher z it extrapolates above the result of Eq. 2.

The radio flux is given by

$$S_r = f(0.148 \text{ Jy})(1+z)^{1+\alpha_r} \left(\frac{\nu}{8.4 \text{ GHz}} \right)^{\alpha_r} \left[\frac{d_L(z_{\text{Arp}})}{d_L(z)} \right]^2 \quad (4)$$

which is normalized to the measured 8.4 GHz flux for Arp 220 from Condon et al. (1991). Since both S_s and S_r depend linearly on the star formation rate, the scale factor f is the same. In local star forming galaxies there is an observed spectral flattening at 1.4 GHz due to free-free absorption (Condon 1992). Since 1.4 GHz measurements at higher redshifts sample higher frequencies that are not sensitive to these absorption effects, we adopt the standard value $\alpha_r = -0.8$ from Condon (1992) to extrapolate local 8.4 GHz fluxes to 1.4 GHz fluxes, in order to be consistent with high redshift observations.

The ratio of Eqs. 3 and 4 with $T_d = 47 \text{ K}$ gives

$$\frac{S_{353 \text{ GHz}}}{S_{1.4 \text{ GHz}}} = 1.1 \times (1+z)^{3.8} \quad (5)$$

A relation of this type was obtained by CY99 based on the SED of M82. In their relation, the factor of 1.1 in Eq. 5 is replaced by 0.25 and the power-law index $\alpha_s - \alpha_r = 3.8$ is replaced by 4.3. However, M82, with more than an order of magnitude lower luminosity than Arp 220 ($L_{\text{FIR}} = 1.78 \times 10^{10} h_{65} \text{ L}_\odot$; Hughes, Dunlop, & Rawlings 1997), is not a ULIG, and so we would argue that our result is more appropriate for the distant submillimeter sources. In addition to their analytic result, CY99

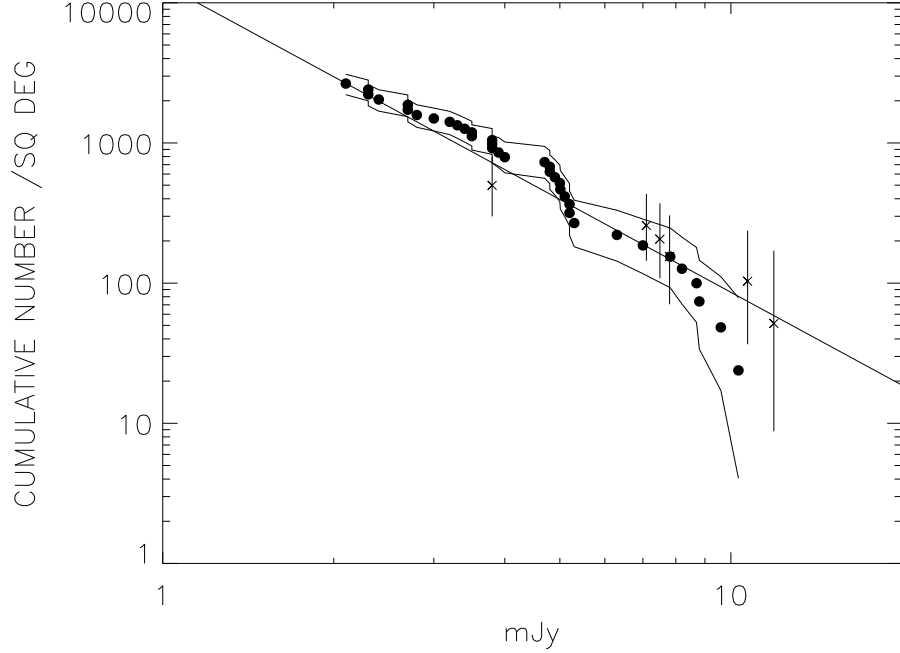


FIG. 4.— Comparison of the radio-selected 850 μm source counts (X symbols with 1σ uncertainties) with the combined counts (solid circles) from blank field submillimeter surveys (H98; Eales et al. 1999; Barger, Cowie, & Sanders 1999). Jagged solid lines are 1σ uncertainties. Solid line is a power-law parameterization, $N(>S) \propto S^{-2.2}$ (Barger, Cowie, & Sanders 1999). Radio selection detects the majority of the bright submillimeter source population.

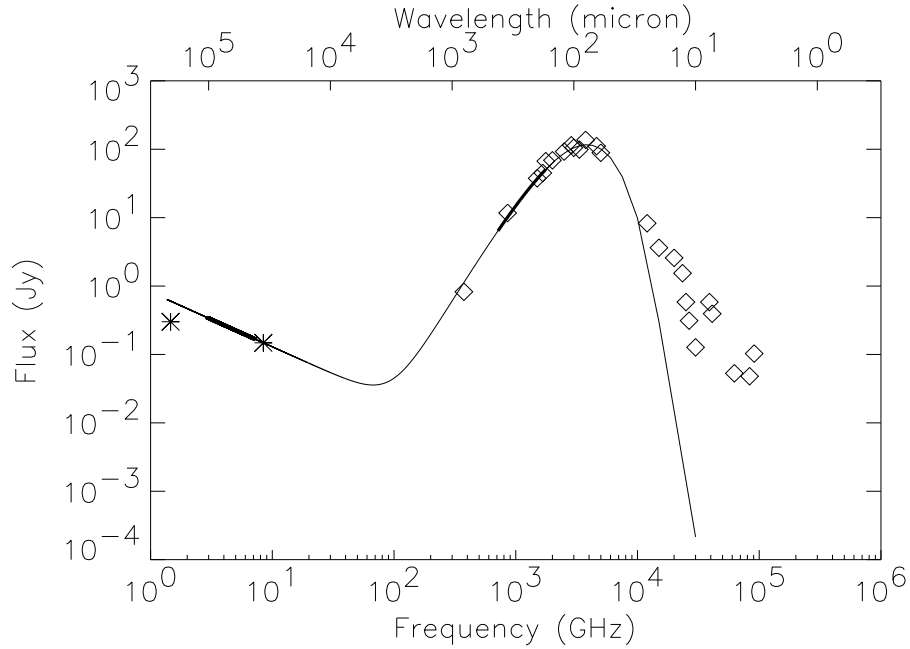


FIG. 5.— Open diamonds are the Arp 220 FIR/submillimeter flux values from Klaas et al. (1997) and Rigopoulou et al. (1996); asterisks are the 1.4 GHz and 8.4 GHz points from Condon et al. (1991). Smooth curve is from Eqs. 3 and 5. Heavy lines indicate the regions of the SED that are sampled over the redshift range $z = 1 - 4$ and illustrate the opposing spectral slopes.

give empirical results for the flux ratio versus redshift for both Arp 220 and M82. Other authors have used the span of the four CY99 curves in their Fig. 1 to estimate redshift ranges; however, the use of M82 again introduces an inappropriate uncertainty in obtaining redshifts.

Inverting Eq. 5, the value of z can be related to the flux ratio by

$$z + 1 = 0.98 \times \left(\frac{S_{353 \text{ GHz}}}{S_{1.4 \text{ GHz}}} \right)^{0.26} \quad (6)$$

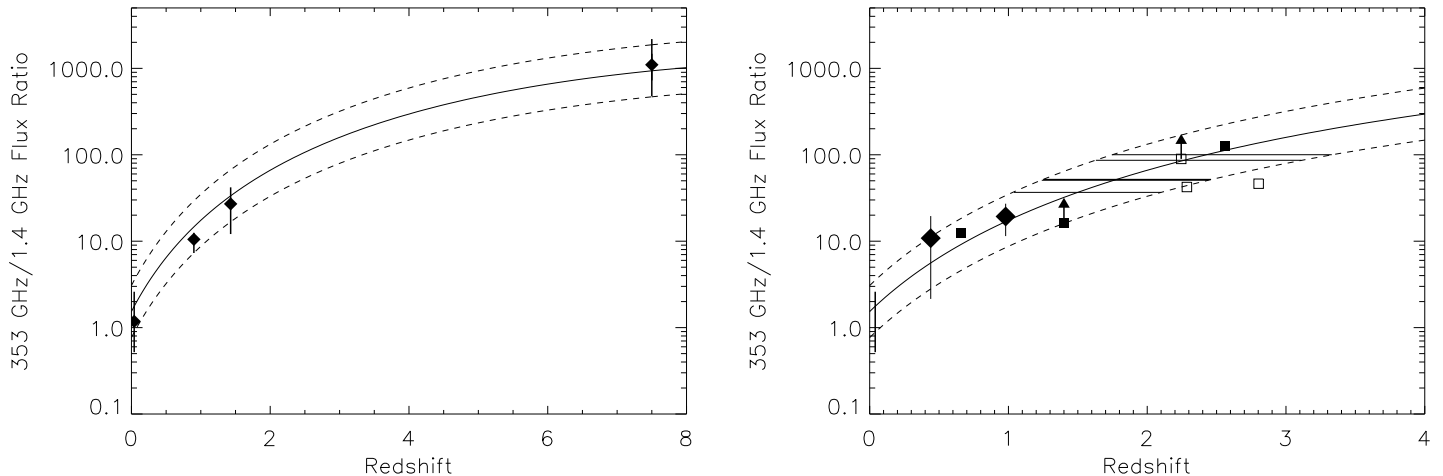


FIG. 6.— (a) Solid curve is the 353 GHz to 1.4 GHz flux ratio versus redshift for a non-evolving redshifted Arp 220. Solid diamonds are the mean values of local ULIG data measured at 3000 GHz ($100\ \mu\text{m}$), 857 GHz ($350\ \mu\text{m}$), 667 GHz ($450\ \mu\text{m}$), and 375 GHz ($800\ \mu\text{m}$) by Rigopoulou et al. (1996) and at 8.4 GHz by Condon et al. (1991). Sources are assumed to be at redshifts 7.5, 1.4, 0.9, and 0.06 to have been observed at 353 GHz ($850\ \mu\text{m}$). 8.4 GHz data were extrapolated to 1.4 GHz at the above redshifts by assuming a synchrotron spectrum with $\alpha_r = -0.8$. Vertical ranges on the measurements are the minimum and maximum flux ratios; the spread is about a multiplicative factor of two, as indicated by the dashed curves. (b) Curves and vertical bar at low redshift are as in (a). Solid squares are individually detected star forming objects from Lilly et al. (1999; CFRS 14 at $z = 0.66$), Dey et al. (1999; HR10 at $z = 1.44$), and Barger et al. (1999b; J1/J2 at $z = 2.56$). Open squares are AGN from Rowan-Robinson et al. (1993; IRAS F10214+4724 at $z = 2.29$), Ivison et al. (1998; L1/L2 at $z = 2.81$), and Ivison et al. (1999; J6/J7 at $z = 2.24$). Large filled diamonds with 1σ uncertainties are average submillimeter-to-radio flux ratios for two redshift bins ($z \leq 0.7$ and $0.7 < z < 1.3$). Short horizontal lines are the redshift ranges for our 6 significant radio-selected submillimeter detections.

which holds for $z \lesssim 3$. For higher redshifts the ratio of Eqs. 2 and 4 must be used. The flux ratio method for estimating redshifts has the advantage that the luminosity distance drops out, and thus there is no dependence on H_0 or on the cosmology.

We make the assumption that unevolved local ULIGs are representative of the distant ULIG population. We show in the following that the Arp 220 SED provides a good representation of the submillimeter-to-radio flux ratios of the ensemble of local ULIGs placed at appropriate redshifts. We use a compilation of submillimeter measurements at 3000, 857, 667, and 375 GHz from Rigopoulou et al. (1996) to infer 353 GHz fluxes at redshifts of 7.5, 1.44, 0.9, and 0.06. Fluxes at 1.4 GHz were extrapolated from the 8.4 GHz measured values of Condon et al. (1991) using a standard synchrotron emission spectrum with $\alpha = -0.8$, as justified earlier. We plot the mean 353 GHz to 1.4 GHz flux ratios versus redshift as solid diamonds in Fig. 6a with ranges from the minimum to maximum flux ratios. The number of objects in the bins are, in order of decreasing redshift, 25, 2, 4, and 7. The data are to be compared with the redshifted Arp 220 flux ratio calculated from Eqs. 2 and 4 and plotted as a solid line in the figure. The spread in measured ratios is about a multiplicative factor of two relative to Arp 220, as indicated by the dashed curves. Thus, the redshifted Arp 220 flux ratio is likely to approximate the flux ratios of ULIGs at high redshifts to this accuracy.

The above conclusion is strengthened by Fig. 6b where we have plotted as solid (star forming galaxies) and open (AGN) squares available submillimeter observations with corresponding radio and redshift information. The star forming galaxies fall neatly on the curves. The average submillimeter-to-radio flux ratio of the galaxies in our sur-

vey which have spectroscopic redshifts and have been observed in the submillimeter are shown in two redshift bins as the large filled diamonds with 1σ uncertainties. The lowest point is consistent with a 3σ null detection, but in the higher redshift bin there is a strong positive detection consistent with the Arp 220 ratio, showing that these objects have cool dust emission and obey the FIR-radio relation at these redshifts. The short horizontal lines show the redshift ranges for our six significant radio-selected submillimeter detections; all are in the $z = 1 - 3$ redshift range. The top portion of Table 3 gives the fluxes and the millimetric redshifts and ranges for these six sources, as well as their bolometric luminosities for both $\Omega_\Lambda = 0$ and $\Omega_\Lambda = 2/3$ (see § 5).

The ULIG sources plotted in Fig. 6 have a range of emissivity indices, β , and dust temperatures in the vicinity of 50 K. It is therefore quite remarkable that all the sources follow a constrained envelope around the Arp 220 submillimeter-to-radio flux ratio. The implication of this empirical correlation is that for practical purposes a temperature-redshift degeneracy (Blain 1999) does not present a serious problem to millimetric redshift estimation.

A recent empirical analysis by Carilli & Yun (2000), which appeared subsequent to the submission of our paper, finds conclusions that are consistent with our analysis above.

5. RADIO AND SUBMILLIMETER FLUXES VERSUS REDSHIFT

In our analysis we assume a flat Universe, $\Omega_M + \Omega_\Lambda = 1$, where Ω_M is the matter density and Ω_Λ the vacuum density. The absolute flux values in Eqs. 2 and 4 depend on the cosmology through the luminosity distance (Carroll,

TABLE 3
SUBMILLIMETER SOURCE REDSHIFTS AND LUMINOSITIES

Catalog #	$S_{353 \text{ GHz}}$ (mJy)	$S_{1.4 \text{ GHz}}$ (mJy)	z_{min}	z	z_{max}	L_{bol} ($10^{12} L_{\odot}$) $\Omega_{\Lambda} = 0$	L_{bol} ($10^{12} L_{\odot}$) $\Omega_{\Lambda} = 2/3$
33	11.9	0.124	1.0	1.5	2.1	5.0	9.1
49	10.7	0.324	1.6	2.3	3.1	4.5	9.0
7	7.8	0.151	1.3	1.8	2.5	3.3	6.3
11	7.5	0.148	1.2	1.8	2.4	3.2	6.0
13	7.1	0.071	1.8	2.4	3.3	3.0	6.0
46 (HDF850.2)	2.4	0.046	1.3	1.8	2.5	1.0	1.9
...	19.0	< 0.040	> 3.6	> 5.0	> 7.6	> 9.2	> 20
...	8.8	< 0.040	> 2.5	> 3.5	> 4.8	> 4.2	> 8.9
(HDF850.1)	5.4	< 0.040	> 2.0	> 2.8	> 3.8	> 2.6	> 5.4

Press, & Turner 1992)

$$d_L(z) = cH_0^{-1}(1+z) \int_0^z dz' / [(1+z')^2(1+\Omega_M z') - z'(2+z')\Omega_{\Lambda}]^{1/2} \quad (7)$$

The basic physics underlying the joint use of radio and submillimeter observations is contained in Figs. 7 and 8. Figure 7 shows predicted Arp 220 radio and submillimeter fluxes versus redshift for the $\Omega_M = 1$, $\Omega_{\Lambda} = 0$ cosmology ($H_0 = 65 \text{ km s}^{-1} \text{ Mpc}^{-1}$) with selected overall strengths $f = 1/3, 1, 3$, and 6 relative to Arp 220. $S_{353 \text{ GHz}}$ is flat with redshift for $z \gtrsim 1$ due to the negative K -correction, whereas $S_{1.4 \text{ GHz}}$ falls sharply with increasing redshift due to the $1/d_L^2$ dependence. These behaviors are characteristic of other cosmologies as well. Thus, radio surveys detect a high proportion of low redshift sources whereas submillimeter surveys offer comparable sensitivity to both moderate ($z \sim 1$) and high redshifts.

In Fig. 8 we illustrate the dependence on cosmology of the absolute fluxes in the $S_{1.4 \text{ GHz}}$ versus $S_{353 \text{ GHz}}$ plane. Figure 8a shows predicted Arp 220 fluxes for the $\Omega_{\Lambda} = 0$ cosmology, and Fig. 8b shows the same for the $\Omega_{\Lambda} = 2/3$ cosmology favored by recent distant supernovae type Ia observations (Perlmutter et al. 1999; Riess et al. 1998). Redshift labels are given on the $f = 1, 3$, and 6 curves. In Fig. 8a the bright submillimeter sources fall near the $f = 3$ contour, indicating that these sources have luminosities several times the luminosity of the Arp 220 prototype. For the $\Omega_{\Lambda} = 2/3$ cosmology we would infer somewhat higher luminosities from the curves, although the redshift estimates remain the same.

From Fig. 8, we see that any submillimeter sources above our detection threshold of 6 mJy would not be detectable in the radio if $z \gtrsim 4$. Of the significant submillimeter sources detected in our survey, two had no radio counterparts and one, HDF850.1, had only a supplemental 8.5 GHz radio detection. Based on the millimetric redshift estimator, these sources are potentially at very high redshift. The bottom three lines of Table 3 give the fluxes and the millimetric redshifts and ranges, along with the

bolometric luminosities for $\Omega_{\Lambda} = 0$ and $\Omega_{\Lambda} = 2/3$, for the three significant SCUBA detections without corresponding 1.4 GHz detections; here the numerical entries are based on the 0.040 mJy (5σ) radio flux limit, which corresponds to the lowest possible redshift and L_{bol} .

Since we have covered only one-third of our ~ 80 square arcminute area with our targeted SCUBA observations, there could in principle be more high redshift submillimeter sources with no radio detections. However, our present radio counts already saturate the bright submillimeter counts distribution from the combined blank field submillimeter surveys (see Fig. 4) and hence argue against the probability of finding many such additional sources.

In contrast, sources of Arp 220 or sub-Arp 220 strength could be seen in the radio but not in the submillimeter with our present 6 mJy threshold if $z \lesssim 2$. Figure 7b shows that we have many such candidates. Our targeted SCUBA observations of optical/NIR-faint radio sources are therefore selecting the high redshift end of the faint radio source population.

6. REST-FRAME COLOR VERSUS REDSHIFT

In Fig. 9 we plot rest-frame AB(2800)–AB(8140) color versus redshift for the radio sample with spectroscopic identifications. The colors of field galaxies in the HDF and SSA22 fields are indicated with tiny solid circles to illustrate how the radio galaxies (solid triangles for sources with $\alpha_r > -0.3$ but otherwise solid circles) generally have very red AB colors. These colors range from ~ 1.5 to ~ 4.5 . There is no evidence for a color trend with redshift. The rest-frame AB colors of the submillimeter galaxies with HK' detections (solid pentagons), although mostly lower limits, are not inconsistent with the colors of the lower-redshift radio sources.

At $z = 2$, AB(2800)–AB(8140) roughly corresponds to AB(I)–AB(HK'), and thus submillimeter sources with similar colors to the radio sources would have observed Vega-based $I - HK'$ colors in the range $3.1 - 6.1$, which would mostly place them in the extremely red object (ERO) category ($I - HK' > 3.7$ or $I - K > 4$; e.g., McCracken et al. 1999 and references therein). This result is

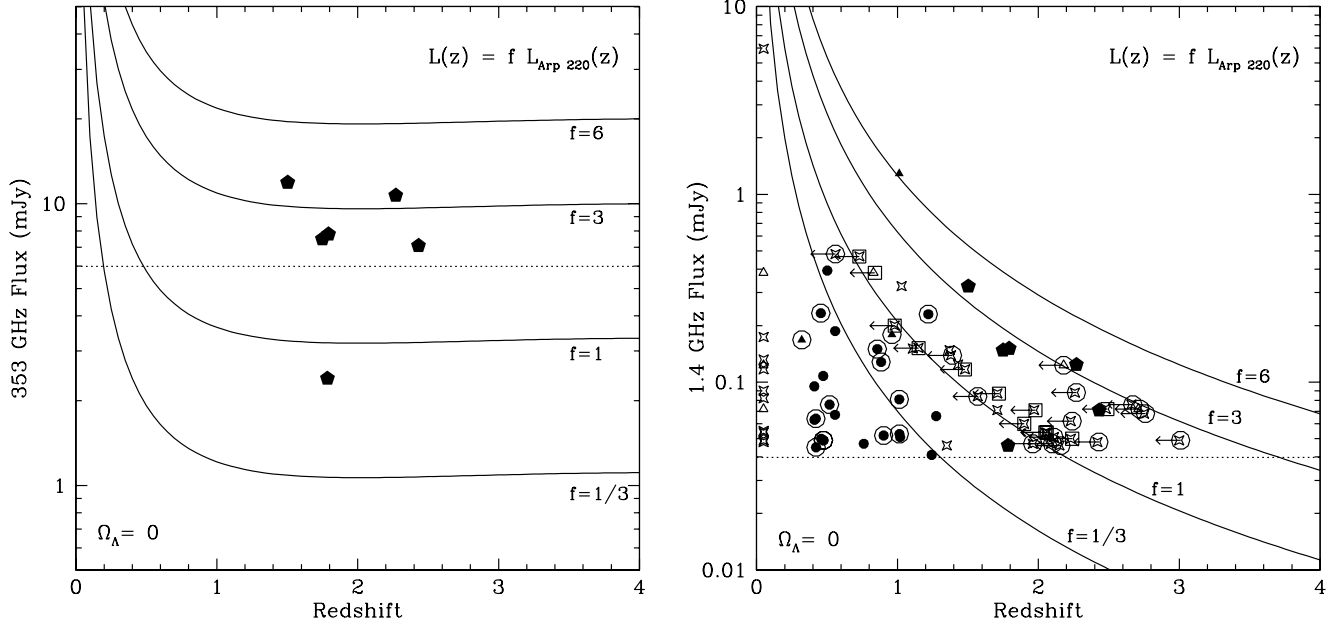


FIG. 7.— (a) Submillimeter flux versus redshift, and (b) radio flux versus redshift for our radio sample. Solid curves show the predicted flux versus redshift for Arp 220 scaled by $f = 1/3, 1, 3$, and 6 . Detection limits of 6 mJy (3σ) for the submillimeter and 0.04 mJy (5σ) for the radio are indicated with dotted lines. Filled circles have spectroscopic redshifts while open crosses do not. Filled (with redshifts) and open triangles have $\alpha_r > -0.3$. Solid pentagons are distant ULIGs at $S_{353} > 6$ mJy (our survey) and $S_{353} < 6$ mJy (H98), shown at their millimetric redshifts. Open squares (optical/NIR-faint) and open circles (optical/NIR-bright) were observed but not detected at 353 GHz at the 6 mJy (3σ) level; millimetric redshift limits from the 1σ upper limits on the submillimeter measurements are indicated by the leftward pointing arrows. Here $\Omega_M = 1$, $\Omega_\Lambda = 0$ with $H_0 = 65$.

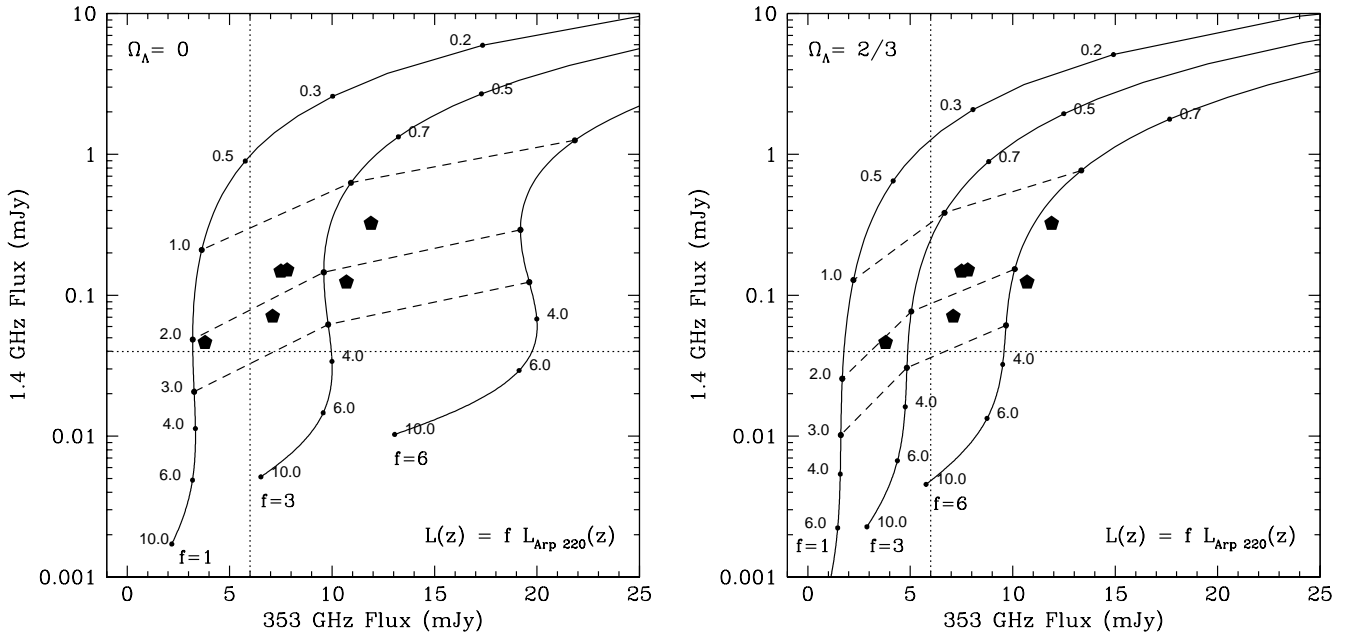


FIG. 8.— Radio versus submillimeter flux for a redshifted Arp 220 SED scaled by $f = 1, 3$, and 6 with (a) $\Omega_M = 1$, $\Omega_\Lambda = 0$, and (b) $\Omega_M = 1/3$, $\Omega_\Lambda = 2/3$. Redshift labels are marked on the curves. Dashed lines connect the curves at constant redshifts of $z = 1, 2$, and 3 . Dotted horizontal line is the 0.04 mJy (5σ) flux limit for the 1.4 GHz sample. Dotted vertical line is the 6 mJy (3σ) limit for our radio-targeted submillimeter survey. Symbols are as in Fig. 7. Approximate redshifts for the sources can be inferred from the curves and are all in the range $z = 1 - 3$, as demarcated in the figure by dashed lines.

consistent with the recent detections of bright ($K < 20$) EROs as submillimeter sources (Cimatti et al. 1998; Dey et al. 1999; Smail et al. 1999a). In general, however, the

submillimeter sources are so optically faint that identifying them as EROs is difficult.

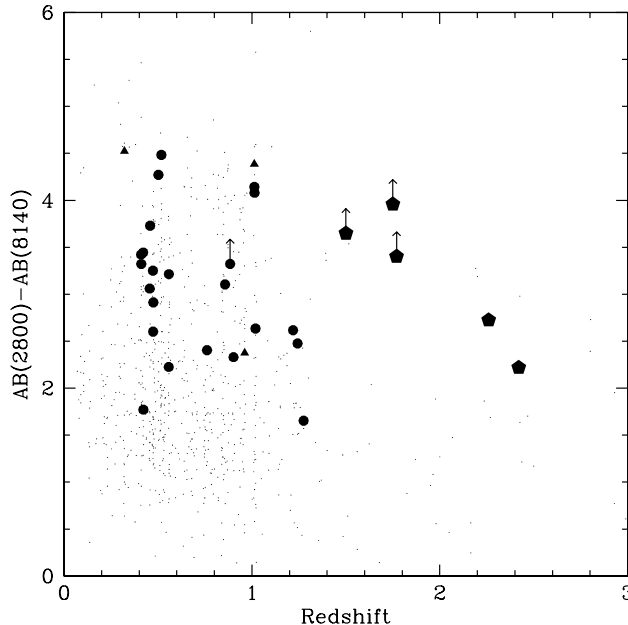


FIG. 9.— $AB(2800)-AB(8140)$ color versus redshift for the 1.4 GHz sources with spectroscopic identifications (solid circles). Solid triangles have $\alpha_r > -0.3$. Solid pentagons are submillimeter sources with HK' detections and millimetric redshift estimates. Tiny circles are from LRIS redshift surveys of the HDF and SSA22 fields and illustrate how much redder the radio sources are than the typical field galaxy.

7. PROPERTIES OF THE RADIO AND SUBMILLIMETER POPULATIONS

The luminosities of our submillimeter sources were obtained by scaling the Arp 220 luminosity at redshift z by the relative source strengths, f ; these are given in Table 3. The FIR luminosity provides a direct measure of the current star formation rate (SFR); with present detection capabilities, the radio provides greater sensitivity to SFRs at low redshifts ($z \lesssim 1.5$) while the submillimeter is superior at high redshifts. In this sense radio and submillimeter data complement each other in getting the SFR over the full range of redshifts. This relative capability is illustrated in Fig. 10 where the strength factors, f , as determined from the radio luminosities relative to redshifted Arp 220 luminosities, are plotted versus redshift in the $\Omega_\Lambda = 0$ cosmology. Here the dotted curve represents the radio threshold of $40 \mu\text{Jy}$, and the solid line at a value of two represents our 6 mJy submillimeter threshold of roughly two times the luminosity of Arp 220 for the $\Omega_\Lambda = 0$ cosmology (see Fig. 8). These two threshold curves cross at $z \sim 2.3$. Since the bulk of the radio detections are at $z \lesssim 1.3$ and have strength factors $f < 1$, their non-detection in the submillimeter is as expected; our $z \sim 2$ sources are detected in both the radio and submillimeter. At redshifts $z \gtrsim 3-4$ the submillimeter may provide the only access to distant ULIGs.

Figure 10 also provides a means to establish the completeness of the ULIG number distribution versus redshift. Our distant ULIG sample is complete over the redshift range $z = 1-3$ (except possibly for the 4 out of 22 optically-faint radio sources that were not observed) because these $z = 1-3$ sources are above both radio and submillimeter detection thresholds. At $z \gtrsim 3$ there is the risk that we may lose sources that fall below the rising 1.4 GHz threshold relative to the Arp 220 luminosity at

redshift z .

7.1. Space Density

The space density of our five significant $S_{850\mu\text{m}} > 6 \text{ mJy}$ submillimeter sources in the redshift range $z = 1-3$ is

$$n = 3.5^{+2.4}_{-1.5} \times 10^{-5}, \quad \Omega_\Lambda = 0 \quad (8a)$$

$$n = 1.1^{+0.7}_{-0.5} \times 10^{-5}, \quad \Omega_\Lambda = 2/3 \quad (8b)$$

in units $h_{65}^3 \text{ Mpc}^{-3}$. In comparison, the space density of local ULIGs ($z < 0.15$; Kim & Sanders 1998) with bolometric luminosities above $10^{12} h_{65}^{-2} L_\odot$ is only $1.7 \times 10^{-7} h_{65}^3 \text{ Mpc}^{-3}$ for $\Omega_\Lambda = 0$ and $1.4 \times 10^{-7} h_{65}^3 \text{ Mpc}^{-3}$ for $\Omega_\Lambda = 2/3$, about a factor of 200 and 80 lower than our high redshift results. The discrepancy in space density is still larger if we compare with local ULIGs that are comparably luminous to the $> 6 \text{ mJy}$ population. Thus, enormous evolution in the ULIG population must take place between $z \sim 2$ and the present.

It is interesting to note a possible empirical similarity between the redshift distribution of quasars and that of submillimeter sources, which might be expected if quasars are a successor stage to merger processes forming submillimeter sources (Sanders & Mirabel 1996). The relative space density of a complete radio-selected quasar sample (Shaver et al. 1998), which should be unaffected by dust obscuration, is approximately described by a Gaussian as a function of redshift, given by

$$n(z) \propto e^{-(z-2.28)^2/1.72} \quad (9)$$

The peaking of this distribution at $z \sim 2.3$ and the rapid fall-off at low redshift seems consistent with our measured submillimeter redshift distribution. Recent ROSAT X-ray

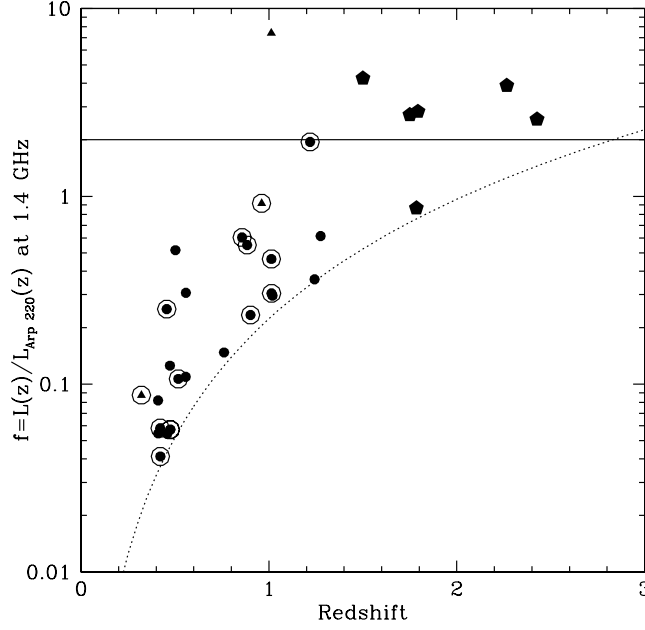


FIG. 10.— 1.4 GHz source luminosity, relative to the redshifted 1.4 GHz luminosity of Arp 220, versus redshift in the $\Omega_\Lambda = 0$ cosmology for the sources that have been spectroscopically observed. The dotted curve represents the radio threshold of $40 \mu\text{Jy}$. The solid curve at a value of two denotes our 6 mJy submillimeter survey's effective minimum sensitivity to sources that have two times the luminosity of Arp 220; the submillimeter source lying below this value is HDF850.2 of H98. The symbols are as in Fig. 7.

studies have found a very high redshift tail ($z \sim 4$) to the quasar distribution that may be above the Gaussian expectation (Hasinger 1998). Since the ROSAT sources were not seen in the optical, it is plausible that they are dust obscured. Similarly, we have found a few submillimeter sources that plausibly lie at $z \gtrsim 3$.

7.2. Conversion from Luminosity to Star Formation Rate

The observed ultraviolet light can most simply be translated to a metal production rate where, as first pointed out in Cowie (1988), there is an extremely tight relation since both metals and ultraviolet light are produced by the same massive stars. However, it is usual (particularly in the FIR) to translate the metal production rate to a total stellar mass production rate, which may be more intuitively interpreted. Unfortunately, this extrapolation requires knowledge of the shape of the initial mass function (IMF), which is quite uncertain.

In the following we shall assume a Salpeter IMF ($\psi(M) \propto M^{-2.35}$, $0.1 - 125 M_\odot$). The SFR is related to the rest-frame 2800 Å luminosity per unit frequency by

$$\dot{M} = \phi \times L_{2800} \quad (10)$$

with L_{2800} in $\text{ergs s}^{-1} \text{Hz}^{-1}$ and \dot{M} in $M_\odot \text{yr}^{-1}$. The Cowie (1988) estimate of ϕ from nucleosynthesis arguments and galaxy SED modelling is 2.2×10^{-28} for the above IMF limits. Later Songaila, Cowie, & Lilly (1989) suggested that ϕ should be about a factor 1.7 lower based on stellar synthesis. Madau et al. (1996) obtained a value of 1.5×10^{-28} based on the evolutionary models of Bruzual & Charlot (1993). The relatively invariant estimates of ϕ are a direct consequence of the nucleosynthesis arguments underlying the modelling; the primary uncertainty in \dot{M} lies in the stellar IMF. We adopt the Madau et al. value

for consistency with other recent papers that follow this normalization. In terms of the solar luminosity, the SFR relation is then

$$\dot{M} = \Phi \times \nu L_{2800} / L_\odot \quad (11)$$

where $\Phi = 5.3 \times 10^{-10}$.

The conversion of the bolometric luminosity to a total stellar mass production rate is an even more invariant prediction of the nucleosynthesis arguments since knowledge of the exact shape of the ultraviolet SED of the galaxies is not needed. The bolometric luminosity in units of the solar luminosity is

$$L_{bol} = BC \times \nu L_{2800} / L_\odot \quad (12)$$

where BC is the bolometric correction. For a flat S_ν over the wavelength range 912 Å to 22000 Å, $BC = 2.95$. Rowan-Robinson et al. (1997) computed a bolometric correction of 3.5 from the Bruzual & Charlot (1993) models, which we adopt. Then the SFR is related to L_{bol} by

$$\dot{M} = (\Phi / BC) \times (L_{bol} / L_\odot) = 1.5 \times 10^{-10} \times L_{bol} / L_\odot \quad (13)$$

\dot{M} would be increased by a factor of 3.3 if we had instead assumed a Miller-Scalo IMF over the same mass range.

Equations 11 and 13 therefore provide a self-consistent description of the mass production rates seen in the optical and submillimeter. Light which directly escapes the galaxy can be mapped with the ultraviolet light, while reprocessed light, which escapes the galaxy in the submillimeter, can be calibrated with Eq. 13.

We now use the Arp 220 bolometric luminosity $L_{bol} = 1.36 \times 10^{12} h_{65}^{-2} L_\odot$ (Klaas et al. 1997) and the 8.4

GHz radio flux of 0.148 Jy (Condon et al. 1991) to calibrate the SFRs for our radio sources. We find $\dot{M} = 200 h_{65}^{-2} M_{\odot} \text{ yr}^{-1}$; thus

$$\dot{M} = L_{8.4 \text{ GHz}}/6.4 \times 10^{27} \quad (14)$$

where the normalization factor is in units of $\text{ergs s}^{-1} \text{ Hz}^{-1}$. From the equations of Condon (1992) translated to the same assumptions about the IMF, we would obtain a normalization of approximately 1.8×10^{27} or about a factor of 3.5 smaller than our result. Our normalization translated with the $\nu^{-0.8}$ spectral shape to 1.4 GHz is

$$\dot{M} = L_{1.4 \text{ GHz}}/2.7 \times 10^{28} \quad (15)$$

7.3. Contribution of the Radio and Submillimeter Sources to the Star Formation Rate Density

Using Eq. 15, we can convert our radio luminosities into SFRDs. We know that 95 per cent of the micro-Jansky radio sources in the HDF region have been resolved at $0.2''$ resolution with the Multi-Element Radio Linked Interferometer (MERLIN) at 1.4 GHz. The median angular size for the radio emission is $1'' - 2''$ (Richards 1999a), which suggests radio emission on galactic or sub-galactic size scales. Thus, the radio emission in most of these systems may originate primarily from star formation, although we cannot exclude contributions to the radio flux densities from embedded AGN.

We divide our radio sources with spectroscopic redshifts into two bins, $0.1 < z \leq 0.7$ and $0.7 < z \leq 1.3$, excluding sources with radio spectral indices $\alpha_r > -0.3$ that might be AGN. Of the 38 presumed star forming objects with $HK' < 20$ in our sample, 23 have spectroscopic redshifts. Most of the remaining 15 sources have not been observed and thus may be expected to follow the same redshift distribution as the identified sources. We therefore calculate the differential comoving volume over a survey area $(23/38) \times 79.4 \text{ arcmin}^2$. The volume is integrated from z_{min} , the lower redshift limit of the bin, to z_{max} , either the radio luminosity limit of the survey or the upper redshift limit of the bin, whichever is smaller. The comoving volume element in Mpc^3 is

$$\Delta V = \frac{1}{3} \times A \times 8.46 \times 10^{-8} \times \left[\left(\frac{d_L(z_{max})}{1 + z_{max}} \right)^3 - \left(\frac{d_L(z_{min})}{1 + z_{min}} \right)^3 \right] \quad (16)$$

where A is the area in arcmin^2 and d_L is in Mpc.

We find that for the $0.1 < z \leq 0.7$ bin, the SFRD in units $h_{65} M_{\odot} \text{ yr}^{-1} \text{ Mpc}^{-3}$ is

$$\text{SFRD} = 0.033^{+0.012}_{-0.009}, \quad \Omega_{\Lambda} = 0 \quad (17a)$$

$$\text{SFRD} = 0.025^{+0.009}_{-0.007}, \quad \Omega_{\Lambda} = 2/3 \quad (17b)$$

and for the $0.7 < z \leq 1.3$ bin,

$$\text{SFRD} = 0.048^{+0.020}_{-0.015}, \quad \Omega_{\Lambda} = 0 \quad (18a)$$

$$\text{SFRD} = 0.032^{+0.014}_{-0.010}, \quad \Omega_{\Lambda} = 2/3 \quad (18b)$$

where the uncertainties are Poissonian based on the number of sources. These represent lower limits to the SFRD since we have not attempted to correct for the contributions of faint sources below our flux limits.

The SFRD from our submillimeter sources can be estimated under the assumption that star formation dominates AGN contributions. We can calculate the contribution of the $S_{850\mu\text{m}} > 6 \text{ mJy}$ submillimeter sources at $z = 1 - 3$ to the SFRD using Eq. 13; we find

$$\text{SFRD} = 0.023^{+0.016}_{-0.010}, \quad \Omega_{\Lambda} = 0 \quad (19a)$$

$$\text{SFRD} = 0.014^{+0.009}_{-0.006}, \quad \Omega_{\Lambda} = 2/3 \quad (19b)$$

Unlike the number distribution versus redshift, the SFRD needs large corrections for completeness due to the fact that we are detecting only relatively bright sources here (at about six times the luminosity at which the submillimeter background is primarily resolved), and the distribution dN/dS increases rapidly as S decreases. To estimate the completeness correction, we assume that the dependences of N on S and z factorize, $d^2N/dSdz = g(S)h(z)$. This is a plausible assumption in the submillimeter where the fluxes are nearly independent of redshift; nonetheless, in view of the Smail et al. (1999b) study, this assumption remains to be confirmed.

We can determine the completeness correction for the SFRD using the empirical number distribution at $850 \mu\text{m}$ versus S

$$dN/dS = 3.0 \times 10^4 \text{ deg}^{-2} \text{ mJy}^{-1}/S^{3.2} \quad (20)$$

that describes the measured submillimeter counts above 2 mJy (Barger, Cowie, & Sanders 1999). We are making the assumption that the flux to L_{FIR} conversion based on Arp 220 applies in the low submillimeter flux region; the justification is that even the dominant $\sim 1 \text{ mJy}$ population are near-ULIG sources. The completeness correction over all submillimeter fluxes is therefore the measured $850 \mu\text{m}$ extragalactic background light (EBL) divided by the $850 \mu\text{m}$ light above 6 mJy. The $850 \mu\text{m}$ EBL measurement of $3.1 \times 10^4 \text{ mJy deg}^{-2}$ from Puget et al. (1996) and $4.4 \times 10^4 \text{ mJy deg}^{-2}$ from Fixsen et al. (1998) imply correction factors in the submillimeter of 11 and 15, respectively. Thus, the estimated total submillimeter contribution to the SFRD in units of $h_{65} M_{\odot} \text{ yr}^{-1} \text{ Mpc}^{-3}$ is

$$\text{SFRD} = 0.25^{+0.17}_{-0.11}, \quad \Omega_{\Lambda} = 0 \quad (21a)$$

$$\text{SFRD} = 0.15^{+0.10}_{-0.06}, \quad \Omega_{\Lambda} = 2/3 \quad (21b)$$

where we have used the factor of 11 completeness correction.

More speculatively, we can determine the SFRD from higher redshift sources using our two $> 6 \text{ mJy}$ submillimeter sources without radio counterparts. In this case we use the volume from $z = 3 - 6$ and the actual area surveyed in the submillimeter. We find

$$\text{SFRD} = 0.029^{+0.038}_{-0.019}, \quad \Omega_{\Lambda} = 0 \quad (22a)$$

$$\text{SFRD} = 0.016^{+0.022}_{-0.011}, \quad \Omega_{\Lambda} = 2/3 \quad (22b)$$

After including the factor of 11 completeness correction, this becomes

$$\text{SFRD} = 0.32^{+0.42}_{-0.20}, \quad \Omega_{\Lambda} = 0 \quad (23a)$$

$$\text{SFRD} = 0.18^{+0.24}_{-0.12}, \quad \Omega_{\Lambda} = 2/3 \quad (23b)$$

H98 used photometric redshift estimates to infer that four of their five $S_{850\mu\text{m}} > 2$ mJy sources were in the redshift range $z = 2 - 4$. While these source identifications were problematic, it appears likely from the present work that the redshifts do lie in this rough redshift range. Using our parameters and a scaled Arp 220 SED, we find that the SFRD for their sources with $\Omega_{\Lambda} = 0$ is $0.10^{+0.08}_{-0.05} h_{65} \text{ M}_{\odot} \text{ yr}^{-1} \text{ Mpc}^{-3}$. If we make a completeness correction to include the contribution below 2 mJy, we obtain $\text{SFRD} = 0.28^{+0.22}_{-0.14} h_{65} \text{ M}_{\odot} \text{ yr}^{-1} \text{ Mpc}^{-3}$, in good agreement with our result in Eq. 21a.

The presence of a substantial fraction of AGN-dominated ULIG sources would reduce the above SFRDs. In a recent near-infrared spectroscopic study of 64 local ULIGs, Veilleux, Sanders, & Kim (1999) found AGN characteristics in 20 – 25 per cent of the sample, which increased to 35 – 50 per cent for the sample with $L_{\text{IR}} > 10^{12.3} L_{\odot}$. Thus, our > 6 mJy contributions to the SFRD may need to be reduced by a factor $\sim 1.5 - 2$. However, the lower AGN fraction in fainter ULIGs seen locally suggests that AGN contamination may be less of an issue for the extrapolated SFRD of the whole submillimeter population.

7.4. Comparison with the Optical Star Formation Rate Density Diagram

The determination of the SFRD from optical observations has been a subject of intense investigation. Observations first indicated a rather rapid rise in the SFRD from $z = 0 - 1$ followed by a sharp decline at higher redshifts with the peak SFRD being $z \sim 1.5$ (Madau et al. 1996). A recent modification in the inferred optical SFRD at low redshifts was made by Cowie, Songaila, & Barger (1999), whose data indicated a more gradual rise in the SFRD than had previously been found by Lilly et al. (1996).

It was realized that dust obscuration effects could result in factors of 3 to 5 (Pettini et al. 1997; Meurer, Heckman, & Calzetti 1999) increases in the SFRD at high redshift. With these rather uncertain dust corrections taken into account, it has been argued that the SFRD flattens at a constant $\text{SFRD} \approx 0.2 h_{65} \text{ M}_{\odot} \text{ yr}^{-1} \text{ Mpc}^{-3}$ in the $\Omega_{\Lambda} = 0$ cosmology for $z = 1 - 5$ (Steidel et al. 1999).

In Fig. 11 we compare the star formation history in the optical (without extinction corrections) with that which we obtain in the submillimeter both before (Eqs. 19a and 22a; solid triangles) and after (Eqs. 21a and 23a; solid circles) correcting for incompleteness. We also include our newly determined radio SFRD limits (Eqs. 17a and 18a) on the figure as solid squares.

The submillimeter contribution to the SFRD inferred from our > 6 mJy observations is comparable to the ultraviolet/optical contribution to the SFRD. The two wavelength regimes are likely sampling different stages in galaxy formation. The submillimeter detects the formation of massive spheroids while the ultraviolet/optical detects the formation of smaller disk or bulge systems. The approximate equality of the optical and submillimeter backgrounds supports this hypothesis; the metal density in present-day disks is roughly comparable to that in the spheroidal components of galaxies, so comparable amounts of light are expected to be produced in their formation (Cowie 1988).

The completeness-corrected submillimeter SFRD, shown by the solid circles in Fig. 11, is based on the assumption that fainter submillimeter sources have the same redshift distribution and properties as the > 6 mJy sample. Hence the SFRD from the entire population contributing to the submillimeter background is about an order of magnitude higher than the extinction-uncorrected ultraviolet/optical SFRD. Since the submillimeter measures reradiated optical light, the observed ultraviolet/optical SFRD contribution should be added to the submillimeter contribution.

We also plot in Fig. 11 the SFRD determined from the sum of the SFRD of the local ULIG data ($z < 0.15$; $L_{\text{bol}} > 10^{12} h_{65}^{-2} L_{\odot}$) from Kim & Sanders (1998) and the local near-ULIG data ($z < 0.02$; $2 \times 10^{11} h_{65}^{-2} L_{\odot} < L_{\text{bol}} < 10^{12} h_{65}^{-2} L_{\odot}$) from Sanders et al. (in preparation). The latter L_{bol} selection is imposed in order to be able to compare with our completeness-corrected submillimeter data points, which should include all sources with luminosities $L_{\text{bol}} > 2 \times 10^{11} h_{65}^{-2} L_{\odot}$. We note that the radio data in Fig. 11 cannot be straightforwardly compared to the ULIG data because the radio sources may not satisfy the same luminosity criteria.

The completeness-corrected SFRD in Fig. 11 shows a very rapid evolution, $\approx (1+z)^6$, in the SFRD of ULIGs from $z \sim 0$ to $z \sim 1 - 3$. Fast evolution is not surprising if the distant submillimeter sources are associated with major merger events giving rise to the formation of massive spheroidal systems (Smail et al. 1998; Eales et al. 1999; Lilly et al. 1999; Trentham et al. 1999). Barger, Cowie, & Sanders (1999) showed that the volume density of submillimeter sources at high redshift ($n = 5 \times 10^{-3} h_{65}^3 \text{ Mpc}^{-3}$ for $q_0 = 0.5$) is comparable to the volume density of present-day elliptical galaxies ($n = 10^{-3} h_{65}^3 \text{ Mpc}^{-3}$).

8. CONCLUSIONS

We have carried out an observational program designed to establish the overlap between the optical/NIR-faint radio population and the submillimeter population and to exploit the complementary information that the radio and submillimeter wavelengths provide to gain insights into the evolution of the galaxy populations. Our major conclusions are as follows

- We have found that submillimeter sources at bright flux levels (> 6 mJy) are associated with optical/NIR-faint radio sources ($40 - 300 \mu\text{Jy}$). This association provides a powerful means to conduct submillimeter surveys by pre-selecting potential bright submillimeter sources through high-resolution deep radio maps.

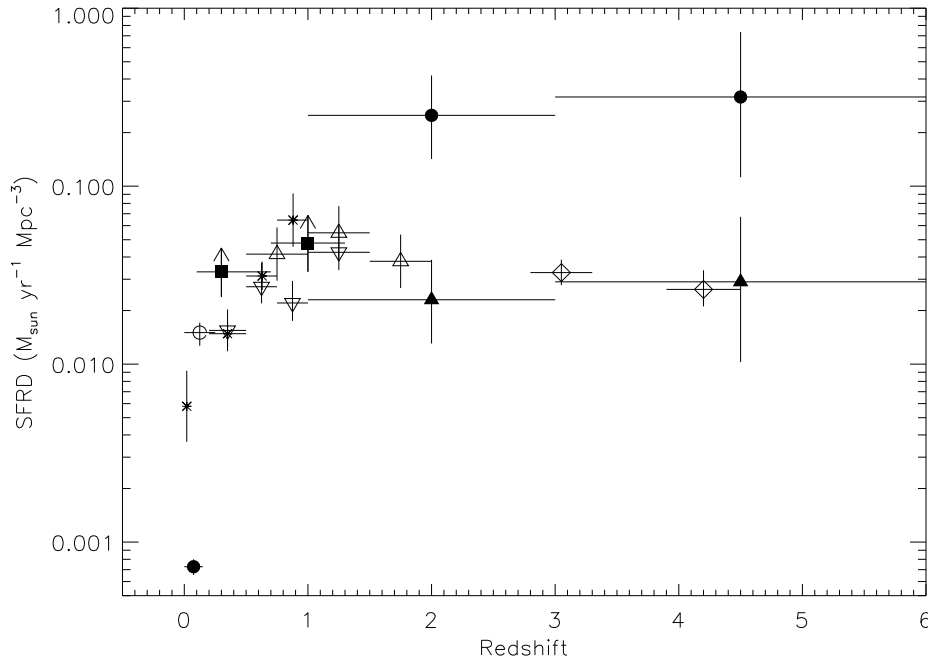


FIG. 11.— SFRD versus redshift for an $\Omega_M = 1$, $\Omega_\Lambda = 0$ cosmology with $H_o = 65$. Our submillimeter results for fluxes > 6 mJy are shown as solid triangles, and the results corrected for completeness are shown as solid circles. Our radio results are shown as filled squares. The uncertainties are Poissonian based on the number of sources. The local point (solid circle) is based on ULIG data from Kim & Sanders (1998) and near-ULIG data from Sanders et al. (in preparation). The open square is from Treyer et al. (1998), asterisks from Lilly et al. (1996), open upside-down triangles from Cowie, Songaila, & Barger (1999), open triangles from Connolly et al. (1997), and open diamonds from Steidel et al. (1999). All optical and ultraviolet points are uncorrected for extinction, as described in the text.

- We have shown that the redshifted submillimeter-to-radio flux ratio of an unevolved Arp 220 SED reproduces the ensemble of local ULIG data placed at appropriate redshifts, and thus Arp 220 provides a prototype for ULIG sources at high redshift. From the Arp 220 model we have derived a *millimetric* redshift estimator to determine the redshifts of the submillimeter sources using the ratio of the submillimeter to radio fluxes. Our estimator is consistent with another recent study by Carilli & Yun (2000). The flux strengths relative to the redshifted Arp 220 SED indicate that the $z = 1 - 3$ bright (> 6 mJy) submillimeter sources are $\sim 3\times$ the luminosity of Arp 220 for $q_o = 0.5$ and $\sim 6\times$ the luminosity of Arp 220 for Λ -dominated models.

- Through radio versus submillimeter flux plots of the Arp 220 predictions with redshift, we have shown that our present survey is sensitive only to sources with strengths comparable to or greater than Arp 220 and that our $40 \mu\text{Jy}$ radio threshold precludes the detection of very high redshift sources ($z > 4$) if they are radio sources; however, we serendipitously observed two bright submillimeter sources without radio detections that may lie at extreme redshifts. An alternate possibility is that they could be colder galaxies than Arp 220 located at $z < 4$. It remains to be established whether the very faint radio population down to $1 \mu\text{Jy}$ have submillimeter counterparts.

- At $z \lesssim 1$ the ultraviolet/optical contribution to the SFRD dominates. At $z > 1$ the submillimeter contribution from > 6 mJy sources is comparable to the observed ultraviolet/optical contribution. The ultraviolet/optical and bright submillimeter are likely sampling two different stages in galaxy formation. The bright submillimeter detects the formation of massive spheroids while the ultraviolet/optical detects the formation of smaller disk or bulge systems.

Joint radio/submillimeter surveys are a powerful way to explore dust-obscured galaxies in the distant Universe since the radio and submillimeter approaches are complementary and allow us to infer redshifts and SFRDs for galaxy sources that we now conclusively see are inaccessible in shorter wavelength observations.

We thank Dave Sanders for valuable discussions, Nicolas Biver for expert observing assistance, and an anonymous referee for helpful comments about the manuscript. Support for this work was provided by NASA through Hubble Fellowship grants HF-01117.01-99A and HF-01123.01-99A awarded by the Space Telescope Science Institute, which is operated by the Association of Universities for Research in Astronomy, Inc., for NASA under contract NAS 5-26555.

REFERENCES

- Aussel, H., Cesarsky, C.J., Elbaz, D., Starck, J.L. 1999, *Astronomy & Astrophysics*, 342, 313
- Barger, A.J., Cowie, L.L., Sanders, D.B., Fulton, E., Taniguchi, Y., Sato, Y., Kawara, K., Okuda, H. 1998, *Nature*, 394, 248
- Barger, A.J., Cowie, L.L., Trentham, N., Fulton, E., Hu, E.M., Songaila, A., Hall, D. 1999a, *AJ*, 117, 102
- Barger, A.J., Cowie, L.L., Sanders, D.B. 1999, *ApJ*, 518, L5
- Barger, A.J., Cowie, L.L., Smail, I., Ivison, R.J., Blain, A.W., Kneib, J.-P. 1999b, *AJ*, 117, 2656
- Blain, A.W., Kneib, J.-P., Ivison, R.J., Smail, I. 1999a, *ApJ*, 512, L87
- Blain, A.W., Smail, I., Ivison, R.J., Kneib, J.-P. 1999b, *MNRAS*, 302, 632
- Blain, A.W., Jameson, A., Smail, I., Longair, M., Kneib, J.-P., Ivison, R.J. 1999c, *MNRAS*, 309, 715
- Blain, A.W. 1999, *MNRAS*, 309, 955
- Bruzual, A.G., Charlot, S. 1993, *ApJ*, 405, 538
- Carilli, C.L., Yun, M.S. 1999, *ApJ*, 513, L13, (CY99)
- Carilli, C.L., Yun, M.S. 2000, *ApJ*, in press, [astro-ph/9910316]
- Carroll, S.M., Press, W.H., Turner, E.L. 1992, *ARA&A*, 30, 499
- Chapman, S.C. et al. 1999, *MNRAS*, submitted, [astro-ph/9909092]
- Cimatti, A., Di Serego Alighieri, S., Vernet, J., Cohen, M., Fosbury, R.A.E. 1998, *ApJ*, 499, L21
- Cohen, J.G., Hogg, D.W., Blandford, R., Cowie, L.L., Hu, E.M., Shopbell, P., Richberg, K. 1999, *ApJ*, submitted
- Condon, J.J., Huang, Z.-P., Yin, Q.F., Thuan, T.X. 1991, *ApJ*, 378, 65
- Condon, J.J. 1992, *ARA&A*, 30, 575
- Connolly, A.J., Szalay, A.S., Dickinson, M., SubbaRao, M.U., Brunner, R.J. 1997, *ApJ*, 486, L11
- Cowie, L.L. 1988, in *The Post-Recombination Universe*, NATO Advanced Science Institute Series, Eds. N. Kaiser, A.N. Lasenby, p. 1
- Cowie, L.L., Gardner, J.P., Hu, E.M., Songaila, A., Hodapp, K.-W., Wainscoat, R.J. 1994, *ApJ*, 434, 114
- Cowie, L.L., Songaila, A., Hu, E.M., Cohen, J.G. 1996, *AJ*, 112, 839
- Cowie, L.L., Hu, E.M. 1998, *AJ*, 115, 1319
- Cowie, L.L., Songaila, A., Barger, A.J. 1999, *AJ*, 118, 603
- Dey, A., Graham, J.R., Ivison, R.J., Smail, I., Wright, G.S., Liu, M.C. 1999, *ApJ*, 519, 610
- Downes, D., Solomon, P.M. 1998, *ApJ*, 507, 615
- Downes, D. et al. 1999, *A&A*, 347, 809
- Eales, S., Lilly, S., Gear, W., Dunne, L., Bond, J.R., Hammer, F., Le Fèvre, O., Crampton, D. 1999, *ApJ*, 515, 518
- Fixsen, D.J., Dwek, E., Mather, J.C., Bennett, C.L., Shafer, R.A. 1998, *ApJ*, 508, 123
- Guiderdoni, B., Bouchet, F.R., Puget, J.-L., Lagache, G., Hivon, E. 1997, *Nature*, 390, 257
- Hasinger G. 1998, *Astron. Nacht.*, 319, 37
- Hauser, M.G. et al. 1998, *ApJ*, 508, 25
- Hodapp, K.-W. et al. 1996, *NewA*, 1, 177
- Holland, W.S. et al. 1999, *MNRAS*, 303, 659
- Hughes, D.H., Dunlop, J.S., Rawlings, S. 1997, *MNRAS*, 289, 766
- Hughes, D.H. et al. 1998, *Nature*, 394, 241, (H98)
- Ivison, R., Smail, I., Le Borgne, J.-F., Blain, A.W., Kneib, J.-P., Bézecourt, J., Kerr, T.H., Davies, J.K. 1998, *MNRAS*, 298, 583
- Ivison, R.J., Smail, I., Barger, A.J., Kneib, J.-P., Blain, A.W., Owen, F.N., Kerr, T.H., Cowie, L.L. 1999, *MNRAS*, in press
- Jenness, T., Lightfoot, J.F. 1998, *Starlink User Note* 216.3
- Kim, D.-C., Sanders, D.B. 1998, *ApJS*, 119, 41
- Klaas, U., Haas, M., Heinrichsen, I., Schulz, B. 1997, *A&A*, 325, L21
- Lagache, G., Abergel, A., Boulanger, F., Désert, F.X., Puget, J.-L. 1999, *A&A*, 344, 322
- Lightfoot, J.F., Jenness, T., Holland, W.S., Gear, W.K. 1998, *SCUBA System Note* 1.2
- Lilly, S.J., Le Fèvre, O., Hammer, F., Crampton, D. 1996, *ApJ*, 460, L1
- Lilly, S.J., Eales, S.A., Gear, W.K.P., Hammer, F., Le Fèvre, O., Crampton, D., Bond, J.R., Dunne, L. 1999, *ApJ*, 518, 641
- Madau, P., Ferguson, H.C., Dickinson, M.E., Giavalisco, M., Steidel, C.C., Fruchter, A. 1996, *MNRAS*, 283, 1388
- Matthews, K., Soifer, B.T. 1994, *Infrared Astronomy with Arrays: the Next Generation*, ed. I. McLean (Dordrecht: Kluwer), p. 239
- McCracken, H.J., Metcalfe, N., Shanks, T., Campos, A., Gardner, J.P., Fong, R. 1999, *MNRAS*, in press
- Meurer, G.R., Heckman, T.M., Lehnert, M.D., Leitherer, C., Lowenthal, J. 1997, *AJ*, 114, 54
- Meurer, G.R., Heckman, T.M., Calzetti, D. 1999, *ApJ*, 521, 64
- Oke, J.B., et al. 1995, *PASP*, 107, 375
- Perlmutter, S. et al. 1999, *ApJ*, 517, 565
- Pettini, M., Kellogg, M., Steidel, C.C., Dickinson, M., Adelberger, K.L., Giavalisco, M. 1998, *ApJ*, 508, 539
- Puget, J.-L., Abergel, A., Bernard, J.-P., Boulanger, F., Burton, W.B., Desert, F.-X., Hartmann, D. 1996, *A&A*, 308, L5
- Richards, E.A., Kellermann, K.I., Fomalont, E.B., Windhorst, R.A., Partridge, R.B. 1998, *AJ*, 116, 1039
- Richards, E.A. 1999a, Ph.D. thesis, University of Virginia
- Richards, E.A. 1999b, *ApJ*, in press, [astro-ph/9908313]
- Richards, E.A., Fomalont, E.B., Kellermann, K.I., Windhorst, R.A., Partridge, R.B., Cowie, L.L., Barger, A.J. 1999, *ApJ*, 526, L71
- Riess, A.G. et al. 1998, *AJ*, 116, 1009
- Rigopoulou, D., Lawrence, A., Rowan-Robinson, M. 1996, *MNRAS*, 278, 1049
- Rowan-Robinson, M. et al. 1993, *MNRAS*, 261, 513
- Rowan-Robinson, M. et al. 1997, *MNRAS*, 289, 490
- Sanders, D.B., Mirabel, I.F. 1996, *ARA&A*, 34, 749
- Schlegel, D.J., Finkbeiner, D.P., Davis, M. 1998, *ApJ*, 500, 525
- Serjeant, S.B.G. et al. 1997, *MNRAS*, 289, 457
- Shaver, P.A., Hook, I.M., Jackson, C.A., Wall, J.V., Kellermann, K.I. 1998, in *Highly Redshifted Radio Lines*, ASP Conf. Series Vol. 156, Eds. C.L. Carilli, S.J.E. Radford, K.M. Menten, G.I. Langston, p. 163
- Smail, I., Ivison, R.J., Blain, A.W. 1997, *ApJ*, 490, L5
- Smail, I., Ivison, R.J., Blain, A.W., Kneib, J.-P. 1998, *ApJ*, 507, 21L
- Smail, I., Ivison, R.J., Kneib, J.-P., Cowie, L.L., Blain, A.W., Barger, A.J., Owen, F.N., Morrison, G. 1999a, *MNRAS*, 308, 1061
- Smail, I., Ivison, R.J., Owen, F.N., Blain, A.W., Kneib, J.-P. 1999b, *ApJ*, in press, [astro-ph/9907083]
- Songaila, A., Cowie, L.L., Lilly, S.J. 1989, *ApJ*, 348, 371
- Steidel, C.C., Adelberger, L., Giavalisco, M., Dickinson, M., Pettini, M. 1999, *ApJ*, 519, 1
- Trentham, N., Blain, A.W., Goldader, J. 1999, *MNRAS*, 305, 61
- Treyer, M.A., Ellis, R.S., Milliard, B., Donas, J., Bridges, T.J. 1998, *MNRAS*, 300, 303
- Veilleux, S., Sanders, D.B., Kim, D.-C. 1999, *ApJ*, 522, 139
- Waddington, I., Windhorst, R.A., Cohen, S.H., Partridge, R.B., Spinrad, H., Stern, D. 1999, *ApJ*, 526, L77

TABLE 1. 1.4 GHz Sample

#	RA(2000)			Dec(2000)			$S_{1.4\text{ GHz}}$ (μJy)	HK'	I	R	V	B	U'	z	$S_{850\text{ }\mu\text{m}}$ (mJy)	$S_{6.75\text{ }\mu\text{m}}$ (mJy)	$S_{15\text{ }\mu\text{m}}$ (mJy)	α_r	
0	12	36	10.57	62	16	51.6	139.0	10.8	20.08	23.80	...	> 26.4	-0.2	2.2
1	12	36	12.48	62	11	40.4	174.0	11.8	16.91	19.09	...	20.67	...	21.70	< -0.89
2	12	36	15.60	62	9	46.8	48.8	8.3	18.77	22.06	...	24.07	...	24.46	...	1.7	3.9
3	12	36	16.15	62	15	13.7	53.9	8.4	> 21.5	24.39	...	25.78	...	> 25.8	...	5.4	1.9
4	12	36	17.08	62	10	11.4	62.0	8.6	18.67	21.58	...	23.92	...	24.28	...	0.6	2.6
5	12	36	17.57	62	15	40.7	20.0	12.8	20.75	23.90	...	24.91	...	25.65	...	-0.3	1.7	...	< -0.55
6	12	36	18.02	62	16	35.3	47.1	8.4	18.04	19.82	...	21.39	...	22.17	...	-0.2	1.5
7	12	36	18.33	62	15	50.5	151.0	11.0	21.36	> 25.3	...	25.58	...	25.05	...	7.8	1.6	...	< -0.63
8	12	36	19.48	62	12	52.6	108.0	9.4	17.49	19.90	...	22.01	...	23.80	0.473	< -0.80
9	12	36	20.28	62	8	44.1	123.0	10.2	18.14	21.53	...	24.91	...	> 25.8	...	3.3	4.9	...	-0.01
10	12	36	21.22	62	11	8.9	52.6	8.2	18.65	22.09	23.51	25.26	...	> 25.8	1.014	4.2	2.9	...	< -0.86
11	12	36	21.27	62	17	8.4	148.0	11.0	21.01	> 25.3	...	> 26.4	...	> 25.8	...	7.5	2.3	...	< -0.56
12	12	36	22.45	62	15	44.5	83.9	8.9	18.07	19.91	...	21.83	...	22.73	...	1.4	1.7	...	< -0.60
13	12	36	22.65	62	16	29.7	70.9	8.7	21.14	23.83	...	25.09	...	25.31	...	7.1	1.7
14	12	36	22.72	62	9	45.9	51.0	8.2	18.47	21.11	...	24.08	...	24.74	...	-2.2	1.9
15	12	36	23.54	62	16	42.7	481.0	25.4	19.48	23.36	...	24.59	...	> 25.8	...	-1.2	1.8	...	-0.63
16	12	36	24.28	62	10	17.0	54.2	8.3	23.39	> 25.3	26.40	> 26.4	...	> 25.8	...	0.3	1.9
17	12	36	29.13	62	10	45.8	81.4	8.7	18.75	22.49	23.83	25.48	26.11	> 25.8	1.013	6.1	2.2	...	< -0.86
18	12	36	30.08	62	9	23.7	46.3	8.2	20.00	22.41	...	25.37	...	> 25.8	...	0.2	1.8
19	12	36	30.46	62	8	51.1	48.0	8.2	19.20	22.57	...	24.87	...	> 25.8	...	-0.5	2.4
20	12	36	31.25	62	9	57.8	152.0	10.9	> 21.5	24.74	26.19	> 26.4	...	> 25.8	...	3.0	1.7	...	< -0.99
21	12	36	32.43	62	16	58.8	81.8	8.9	17.06	19.17	...	21.02	...	22.69
22	12	36	33.74	62	10	6.2	46.5	8.1	18.63	21.66	23.14	23.78	...	24.68	...	0.8	1.7	...	< -0.98
23	12	36	34.46	62	12	13.0	233.0	13.9	16.36	19.09	19.79	21.12	21.74	22.89	0.456	0.1	2.9	...	448.
24	12	36	34.51	62	12	41.0	230.0	13.8	19.10	22.29	23.25	24.22	24.08	24.72	1.219	2.1	2.3	...	363.
25	12	36	35.59	62	14	24.1	87.8	8.8	19.25	22.71	23.45	23.88	24.05	25.30	...	3.9	3.8	...	441.
26	12	36	36.91	62	13	20.4	50.0	7.9	22.29	> 25.3	> 26.6	> 26.4	> 26.6	> 25.8	...	1.7	2.1	...	< -0.87
27	12	36	37.01	62	8	52.4	71.1	8.7	> 21.5	24.47	...	25.77	...	> 25.8	...	2.2	2.3
28	12	36	40.74	62	10	10.6	86.8	8.8	21.22	> 25.3	26.07	> 26.4	...	> 25.8	...	0.3	2.1	...	-0.44
29	12	36	41.55	62	9	48.3	75.8	8.6	17.36	20.21	...	22.80	...	> 25.8	0.518 ^a	0.6	2.3	...	< -0.56
30 ^b	12	36	42.10	62	13	31.4	467.0	24.6	21.23	25.30	26.05	26.05	> 26.6	> 25.8	...	0.7	0.8	...	23.

TABLE 1. (continued)

#	RA(2000)			Dec(2000)			$S_{1.4 \text{ GHz}}$ (μJy)		HK'	I	R	V	B	U'	z	$S_{850 \text{ } \mu\text{m}}$ (mJy)		$S_{6.75 \text{ } \mu\text{m}}$ (mJy)		$S_{15 \text{ } \mu\text{m}}$ (mJy)	α_r
31	12	36	42.22	62	15	45.5	150.0	10.7	18.06	20.86	...	23.30	24.14	25.08	0.857 ^a	-1.1	2.9	...	459.	-0.50	
32 ^b	12	36	44.39	62	11	33.1	1290.0	61.2	17.85	21.04	22.66	24.74	25.57	> 25.8	1.013	0.3	2.1	-0.30	
33	12	36	46.05	62	14	48.7	124.0	9.8	21.65	24.72	25.26	25.86	25.94	> 25.8	...	10.7	2.1	-0.84	
34	12	36	46.33	62	16	29.6	393.0	21.1	18.01	20.20	...	22.75	...	> 25.8	0.502 ^a	< -1.62	
35 ^b	12	36	46.34	62	14	4.7	179.0	11.7	18.36	20.76	22.09	22.86	23.73	24.62	0.961	0.3	1.1	191.	107.	0.04	
36 ^b	12	36	46.70	62	12	26.5	72.0	9.1	> 22.6	> 25.3	> 26.6	> 26.4	> 26.6	> 25.8	...	1.1	0.6	< -1.14	
37	12	36	46.76	62	14	45.5	117.0	9.6	21.00	23.20	23.40	23.60	23.50	24.10	...	0.5	2.1	...	144.	-0.98	
38 ^b	12	36	49.71	62	13	12.8	49.2	7.9	18.74	21.09	21.86	23.04	23.71	25.05	0.475	1.0	0.6	136.	320.	-0.72	
39	12	36	50.20	62	8	44.7	76.4	8.8	17.64	20.01	...	22.04	...	23.92	...	1.1	4.7	< -0.80	
40	12	36	51.13	62	10	30.7	95.0	9.0	17.36	19.88	20.78	21.87	...	23.86	0.410	341.	-0.74	
41 ^b	12	36	51.76	62	12	21.3	49.3	7.9	> 21.5	> 25.3	> 26.6	> 26.4	> 26.6	> 25.8	...	0.1	0.6	...	48.	-0.71	
42	12	36	52.92	62	14	44.0	168.0	11.3	16.52	18.70	19.59	20.71	21.87	24.04	0.321	0.8	2.3	0.12	
43 ^b	12	36	53.40	62	11	39.6	65.7	8.2	19.31	21.88	22.60	23.22	23.00	23.43	1.275	0.0	1.2	...	180.	-0.77	
44	12	36	54.70	62	10	39.6	48.2	8.0	> 21.5	> 25.3	> 26.6	> 26.4	> 26.6	> 25.8	< -1.00	
45	12	36	55.77	62	9	17.4	64.2	8.4	17.80	20.39	...	22.43	...	24.38	0.421 ^a	4.9	3.5	< -0.55	
46 ^b	12	36	56.60	62	12	7.6	46.2	7.9	> 22.6	> 25.3	> 26.6	> 26.4	26.22	> 25.8	...	2.5	0.7	< -1.32	
47 ^b	12	36	56.91	62	13	2.2	49.5	7.9	19.55	22.64	23.86	24.70	24.85	> 25.8	0.474	0.9	0.6	94.	...	< -1.22	
48	12	36	59.95	62	14	49.9	47.0	7.9	18.52	20.92	22.02	22.93	23.53	24.15	0.761	295.	...	
49	12	37	0.26	62	9	9.8	324.0	18.0	20.98	> 25.3	...	> 26.4	...	> 25.8	...	11.9	3.0	-0.89	
50	12	37	1.57	62	11	46.6	128.0	9.9	20.14	24.81	25.73	> 26.4	> 26.6	> 25.8	0.884	4.7	2.1	...	15.	-0.67	
51	12	37	2.76	62	14	1.6	41.4	7.8	18.91	21.89	22.93	23.87	24.22	24.91	1.243	< -0.79	
52	12	37	5.88	62	11	53.6	52.5	8.0	18.18	20.55	21.75	22.63	23.02	23.48	0.902	0.1	1.8	< -1.27	
53	12	37	7.21	62	14	8.1	45.3	7.9	20.29	24.70	25.14	25.92	> 26.6	> 25.8	-0.29	
54	12	37	7.97	62	11	21.5	60.3	8.2	20.76	25.13	26.36	> 26.4	> 26.6	> 25.8	...	-1.2	1.8	< -0.82	
55	12	37	8.16	62	16	59.0	50.4	8.3	17.74	20.17	...	22.22	...	24.76	0.458	
56	12	37	8.32	62	10	56.1	45.1	8.0	17.98	19.87	20.40	21.19	21.70	22.24	0.422	-0.9	1.9	-0.35	
57	12	37	9.45	62	8	37.7	72.0	8.8	17.62	20.47	...	23.43	...	> 25.8	...	5.1	4.6	0.35	
58	12	37	9.77	62	8	41.1	67.9	8.3	18.52	21.46	...	23.81	...	24.27	...	8.3	4.5	
59	12	37	11.34	62	13	31.0	132.0	10.1	19.51	22.66	23.40	24.21	24.64	25.50	-0.69	
60	12	37	11.98	62	13	25.7	53.9	8.1	> 21.5	24.98	25.28	25.42	26.03	> 25.8	< -1.16	
61	12	37	13.59	62	16	3.8	55.3	8.3	20.08	22.90	...	24.95	...	25.29	
62	12	37	16.38	62	15	12.3	187.0	12.2	17.36	19.80	21.96	22.19	22.98	24.10	0.558	-0.41	
63	12	37	16.57	62	16	43.5	66.5	8.7	19.23	22.00	...	23.74	...	24.32	0.557	
64	12	37	16.83	62	10	7.4	63.3	8.5	17.59	19.90	21.05	21.90	...	23.83	0.411	
65	12	37	21.25	62	11	30.0	382.0	24.7	20.90	25.30	...	> 26.4	> 26.6	> 25.8	...	-2.4	2.5	0.28	
66	12	37	21.45	62	13	46.5	50.5	8.2	19.39	22.14	...	24.31	24.57	25.36	1.019	< -0.66	
67	12	37	25.04	62	8	56.5	90.0	9.4	18.65	22.03	...	24.89	
68	12	37	25.29	62	10	6.0	117.0	10.0	17.24	19.35	...	20.95	
69	12	37	25.73	62	11	28.5	5960.0	20.0	> 21.5	25.30	...	26.40	-1.35	

^aThese redshifts are from Cohen et al. (1999)^bSources in our re-reduction of the H98 HDF-proper SCUBA data